Analysis of nonlinear dynamics of fully submerged payload hanging from offshore crane vessel

M.A. Hannan[1, 3], W. Bai[2, 3*]

[1]School of Marine Science and Technology, Newcastle University, Newcastle upon Tyne, UK

[2] School of Computing, Mathematics and Digital Technology, Manchester Metropolitan University, Chester Street, Manchester M1 5GD, UK

[3]Department of Civil and Environmental Engineering, National University of Singapore, Kent Ridge, Singapore 117576, Singapore

Abstract

The nonlinear dynamic responses of a fully submerged payload hanging from a fixed crane vessel are investigated numerically. A three dimensional fully nonlinear time domain model based on the boundary element method is implemented to perform the analysis. Both the payload and fixed crane vessel are considered to be periodically excited by regular waves inside the numerical tank. The motion of the payload is found to exhibit various nonlinear phenomena (for example, sub-harmonic motion, period doubling behavior) due to the presence of fixed crane vessel. Analysis tools such as the phase trajectory, bifurcation diagram and Poincaré map are used to investigate the motion characteristics of this submerged payload which is undergoing constrained pendulum motions in various scenarios. Parametric studies are also performed by varying several design parameters in order to evaluate the sensitivity of the nonlinear phenomena. Different orientations of the crane vessel and submerged payload are also considered and the results obtained reveal several important conclusions concerning the dynamic behavior of the submerged payload of offshore crane vessel during operations. It is found that change of wave motion frequency coupled with various orientations of the floating barge and submerged payload significantly alters the payload motion behavior and introduces various nonlinear phenomena. The present study can be further extended to identify the limits of the operating conditions of floating cranes and to devise techniques to control or damp the unexpected motions of the submerged payload.

* Corresponding author.
E-mail address: w.bai@hotmail.com (W. Bai).

Keywords: Wave structure interaction; Nonlinear dynamics; Crane barge; Submerged payload; Pendulum motion; Phase trajectory and Poincaré map

1. Introduction

Floating cranes are applied for a variety of tasks in offshore areas including transportation, assembling of costly structures and salvage operations. Efficient and safe operations of crane vessels at offshore are thus becoming increasingly important due to the increase in offshore activities particularly in deep water region and with a demand for higher lift capacity. Practical problems arise during crane vessel operations due to the difficulties in positioning accurately the payload being handled, which could result in collisions. Even small disturbances in the state of the system, for example caused by waves of a ship passing by, can entail the danger of collisions of the load with the ship or other objects. Besides, the amplitude of the motion of the hull has to stay small as well, in order to achieve the required positioning accuracy.

There exists considerable amount of literature devoted to the analysis and control of undesired motions of the crane payload hanging in air for example, Patel et al. (1987), McCormick and Witz (1993) ,Witz (1995), Balachandran et al. (1999), Cha et al. (2010). Linearized mathematicl models to describe the dynamics of crane vessel in a wide range of operations are also reported in several papers such as Clauss and Riekert (1989, 1990 and 1992), Clauss and Vannahme (1999). Among these, Clauss and Vannahme (1999) showed that the coupled system of floating crane and swinging load in air shows distinctly nonlinear phenomena and parametric osciallations can occur. They also conculded that under such conditions linear methods can not predict a heavy lift operation as those methods underestimate the occuring loads and motions. Another study performed by Liaw et al. (1992) found that one of the frequently encountered nonlinear behavior, namely sub-harmonic oscialltions of many offshore structures can be attributed to the wave force-structure interaciton. This fact was investigated by them both analytically and experimentally using an articulated tower model.

Ellermann and Kreuzer (1999, 2003) and Ellermann et al. (2002) on the other hand, studied the nonlinear dynamics of floating cranes from more practical point of view. They applied the potential theory to evaluate the dynamic responses of moored crane vessels in regular waves and compared the results with physical experiments.

In the experimental part of their work, moored models of two different crane vessels were excited by regular waves in a wave tank (Ellermann et al. 2002). The hydrodynamic properties (added mass and radiation damping matrices) as well as hydrodynamic exciting forces on both vessels were computed using the software package WAMIT. The theoretical part of the work concerned a multi-degree-of-freedom mathematical modeling of the floating crane vessel where the hull and the payload were represented by rigid bodies. The mathematical description of the moored crane vessel was mainly based on the work of Jiang (1991) which involved the transformation of the frequency-dependent hydrodynamic radiation forces into the time domain by introducing additional state variables. In addition, in this model both the wave-vessel interaction and the hydrodynamic fluid loading on the hull were assumed to be linear so that superposition was applied.

Different mathematical tools have also been used in literature to investigate resonances and sub-harmonic motions, for example in Liaw (1988), Raghthama and Narayanan (2000), Ellermann (2005). The multiple-scale method is used for the analysis in frequency domain and the path following algorithms are applied for a numerical bifurcation analysis (Jiang 1991). In general, periodically forced systems are found to exhibit different nonlinear phenomena ranging from periodic, sub-harmonic or quasi-periodic motion to chaotic behavior. Qualitative changes in the dynamics of the system also arise as parameters are varied. Some of these changes can be considered as critical with respect to the vessel safety and operating limits. Even if not all of these phenomena exist for a specific technical system, they can often be observed for some sets of parameters. With mathematical models of crane vessels including nonlinearities, it is possible to show that period doubling and chaotic behavior occur in the motion of the investigated systems.

As can be seen, all these previous studies so far only considered the behavior of the payload suspended in air. Most of these studies mainly focused on the analysis of crane vessels and ignored the motion of submerged payload in waves, as well as the influence of crane vessel on submerged payload motions. However, understanding of the dynamics of the fully submerged payload under nonlinear wave-structure interactions is quite important in order to ensure safe installation, especially when the payload is quite heavy compared to the vessel displacement. Furthermore, the installation process is a time varying problem and involves the wave interaction with a constantly moving payload. The use of traditional frequency domain analysis to solve this problem, therefore, might not be appropriate to obtain accurate results, because the Taylor series expansion adopted in the frequency domain analysis that expresses the boundary condition on the mean body surface is not applicable.

Therefore, a fully nonlinear time-domain numerical model was adopted in Hannan and Bai (2015) to simulate a submerged moving payload of a crane barge in water waves. The present study is a continuation to the same authors' previous work, but attempts to shed further light on the nonlinear dynamics of the payload. In Hannan and Bai (2015), the general hydrodynamic information, including forces and motions of the submerged payload were reported for different arrangements and scenarios. Whereas, in this work emphasis is given towards the insightful analysis of the nonlinear dynamics of payload motion behavior. Dynamic analysis tools such as the phase trajectory and the Poincaré map are used here to identify the motion characteristics of the suspended heavy submerged payload as it moves laterally or down towards the sea bed while influenced by the nonlinear waves and a fixed crane barge near to it, which is not available in literature till date.

Generally, the phase trajectory and the Poincaré map are widely used to explain the nonlinearity of various engineering systems. Applications of these tools in offshore engineering problems can also be found in literature. For example, Witz et al. (1989) used the Poincaré mapping to identify the region of chaotic motions in response of a semisubmersible to harmonic excitations. Yim and Lin (1991) investigated the rocking behavior and overturning stability of free standing offshore equipment due to support excitations using these techniques, while Lin and Yim (1995) studied the chaotic roll motion and capsize of ships under periodic excitations including random noises. Among more recent studies, Chen et al. (2014) applied the techniques of impact maps, Poincaré maps and phase portraits to explain the motion characteristics of the barge-deck system undergoing vertical impacts with the substructure. Their emphasis was on the modeling of float over installations of offshore structures. Gavassoni et al. (2015) on the other hand, studied nonlinear vibration modes of offshore articulated tower and applied the Poincaré mapping to detect the multiplicity of corresponding stable and unstable modes.

2. Mathematical formulation

A numerical wave tank defined in Fig.1 is considered to simulate the above mentioned wave structure interaction problem. This numerical wave tank involves a wave maker (paddle to generate the wave) at the left end and a damping layer placed on the water surface to avoid the wave reflection from the far right end of the wave tank. The floating barge and its fully submerged cylindrical payload are placed near the middle of the tank. The cylindrical payload, hanging from the crane here is attached to a cable from the top to have constrained motions and subjected to the following nonlinear equation of motion (Bai et al. 2014):

$$-(f_x \cos\xi_5 - f_z \sin\xi_5)L = mL^2 \frac{d^2\xi_5}{dt^2} . \tag{1}$$

Here, m is the mass of the cylindrical body concentrated at its center of mass, and L is the distance between the rigid cable origin and the center of mass of the cylindrical payload. ξ_5 is the angular displacement of the vertical cylinder at the cable origin with respect to the vertical plane, f_x and f_z are the horizontal and vertical dynamic forces on the submerged cylinder respectively.

Two right handed Cartesian coordinate systems are defined. One is a space fixed coordinate system Oxyz having the Oxy plane on the mean free surface and the origin O usually at the center of the crane barge on the Oxy plane. In this case the z axis is positive upwards. The other is a body fixed coordinate system O′$x'y'z'$ with its origin O′ placed at the center of mass of the submerged moving body. When the body is in an upright position, these two sets of coordinate systems are parallel and the center of mass of the submerged body is located at $\mathbf{X}_g = (x_g, y_g, z_g)$ in the space fixed coordinate system.

Fig. 1. Sketch of definition for the numerical model

Based on the assumption that the fluid is incompressible and inviscid, and the flow is irrotational within the fluid domain, potential flow theory can be used to describe this wave–body interaction problem, where a velocity potential $\phi(x, y, z, t)$ satisfies Laplace's equation within the fluid domain Ω,

$$\nabla^2\phi = \frac{\partial^2\phi}{\partial x^2} + \frac{\partial^2\phi}{\partial y^2} + \frac{\partial^2\phi}{\partial z^2} = 0 , \tag{2}$$

and is subject to various boundary conditions on all surfaces of the fluid domain.

On the free water surface S_F, the kinematic and dynamic wave conditions in the Lagrangian description are

$$\frac{D\mathbf{X}}{Dt} = \nabla\phi, \tag{3}$$

$$\frac{D\phi}{Dt} = -gz + \frac{1}{2}\left|\nabla\phi^2\right|. \tag{4}$$

Here, D/Dt is the usual material derivative, $\mathbf{X}$ denotes the position of points on the free surface, and g is the acceleration due to gravity. The kinematic condition on the instantaneous wetted body surface S_B is

$$\frac{\partial\phi}{\partial n} = \mathbf{V_n}, \tag{5}$$

where $\mathbf{V_n}$ is the velocity of the body in the normal direction. If small angular motions are assumed, the motions of a three dimensional rigid body about its centre of mass can be described in terms of six components,

$$\mathbf{V_n} = \left[\dot{\boldsymbol{\chi}} - \dot{\boldsymbol{\alpha}} \times (\mathbf{X} - \mathbf{X_g})\right] \cdot \mathbf{n}, \tag{6}$$

where $\mathbf{n}$ is the normal unit vector pointing out of the fluid domain, $\boldsymbol{\chi} = (\xi_1, \xi_2, \xi_3)$ is a translatory vector denoting the displacements of surge, sway and heave and $\boldsymbol{\alpha} = (\xi_4, \xi_5, \xi_6)$ is a rotational vector indicating the angles of roll, pitch and yaw respectively, about Oxyz and measured in the anticlockwise direction. However, it should be noted that in this study the cylinder is only allowed to have angular motion with respect to the cable origin point. In addition, if a fixed body is considered, the boundary condition on the body surface S_B will become the same as that on the side wall S_w and the horizontal seabed S_D, which is known as the impermeability condition,

$$\frac{\partial\phi}{\partial n} = 0, \tag{7}$$

and the boundary condition on the wave maker can be given as

$$\frac{\partial\phi}{\partial x} = U(t), \tag{8}$$

where $U(t) = a\omega\sin(\omega t)$ is the velocity of the wave maker, a and ω are the corresponding motion amplitude and frequency of the wave maker and this boundary condition is imposed at its instantaneous position. Furthermore, the initial conditions are taken as

$$\phi = 0, \quad z = 0 \text{ when, } t \le 0. \tag{9}$$

The higher-order boundary element method is employed to solve this mixed boundary value problem at each time step, where the surface over which the integral is performed is at first, divided into several patches and each of these patches is discretized by quadratic isoparametric elements. In the present method, structured 8-node quadrilateral meshes are distributed on the vertical solid surfaces including the body surface S_B, wave maker S_{WM} and tank walls S_W. On the free surface S_F and the bottom of the body, unstructured 6-node triangular meshes are generated by using the Delaunay triangulation method.

The mesh is generated for four main configurations of coupled barge and payload system, which are:

- Cylinder Only: a single submerged cylinder subjected to pendulum motions inside the numerical tank and there is no barge nearby.
- Head Sea: barge in head sea (facing the incoming waves in the lengthwise direction) with the submerged cylindrical payload under constrained motions near to it.
- Beam Sea (Up): barge in beam sea (facing the incoming waves in the widthwise direction) with the submerged cylinder under constrained motions near the upstream side of the barge (the wave passes the payload before hitting the barge).
- Beam Sea (Dn): barge in beam sea with the submerged payload under pendulum motions near the downstream side of the barge.

Fig. 2 shows the snapshots of the free surface and body meshes for these 4 main configurations. The waves are coming from the left hand side in these figures and the cylindrical payload here has a radius r = 0.16d and length l = 0.2d, where d is the depth of the numerical tank. All other length parameters in this study are normalized by d, including wave amplitude. The initial lateral gap between the surface of the barge and submerged cylinder is taken as 0.19d. During the simulation, the minimum gap is found to be 0.07d which occurs for the case with cable length 0.8d and wave amplitude 0.015d. Thus, it can be said that the safety margin for a possible collision between the two bodies under the present study condition is around 36% of the initial gap between them. More details regarding the dimensions of numerical tank and floating barge, as well as meshing particulars can be found in Hannan and Bai (2015).

Fig. 2. Mesh generated for various configurations: (a) Cylinder Only; (b) Head Sea; (c) Beam Sea Up; and (d) Beam Sea Dn

The detailed mathematical formulation and numerical implementation of the present problem is also omitted here as these can be found in Bai et al. (2014) as well as in Bai and Eatock Taylor (2006). Several validation studies for simple geometries related to the current study are also presented in those papers.

In the next few sections, this fully nonlinear numerical model is applied to investigate the motion characteristics of the submerged cylindrical payload. The payload is assumed to be connected with the crane tip (point C as marked in Fig. 1) by a rigid cable and is allowed to have pendulum motion about that point only. Parametric studies are performed considering several control parameters namely, motion amplitude and frequency of the wave, length of the cable and moving speed of the payload. In all the studies, the water depth d, gravitational acceleration g and fluid density ρ are taken to be unity to non-dimensionalize other parameters. The density of cylindrical payload is taken as 1.2ρ in order to make it heavier than water, thus ensuring enough tension in the cable to justify the rigid cable assumption.

A number of simulation cases are designed to perform the intended investigation and list of all these cases is provided in Table 1. Test cases modelled for each section are tabulated under the section heading for the ease of reading. For example, under the Cyl only geometric configuration, 11 simulation cases are run (each case for a single frequency, ranging from ω = 1.5 to 2.5 with an increment of 0.1) to study the influence of wave frequency. Here, ω is the wave frequency (rad/s), a is the wave amplitude, Lc is the length of the cable, D represents the vertical distance between the undisturbed free surface level and the cylinder top surface and V_d is the downward moving speed of the payload.

Table 1. List of test cases

3. Nonlinear dynamics of submerged payload under various wave frequencies

The frequency of the incoming waves plays an important role in determining the operating scenario of offshore crane vessel. The response of the submerged payload varies significantly with the change of incoming wave frequency as well as with the change of cylinder positioning along the crane barge. To investigate these issues, several simulations are performed in this section considering different frequencies of the wave maker motion for each of the geometric configurations defined in Fig. 2. All other variables are kept constant during this process.

3.1 Analysis using time histories, phase trajectories and Poincaré map

Among the results obtained, the time histories of pendulum motion of the payload for the Cylinder Only scenario are shown in Fig. 3. These time histories are drawn for three different frequencies and over a selected range of wave periods. As depicted, the motion amplitude decreases with the increase of frequency and a significant influence of low frequency response arises at the same time. These low frequency components are found to arise mainly due to the low frequency wave drift force (Sarkar and Eatock Taylor 1998), the nonlinear interaction between the waves and structures (Hassan et al. 2010), as well as due to the influence of natural frequency of the structure. For submerged payload under pendulum motions, the influence of natural frequency is found to be most prominent as explained in details by Hannan and Bai (2015).

Fig. 3. Time histories of cylinder motion for different wave maker motion frequencies at a = 0.01 and L_c = 0.5d [Cylinder Only]: (a) ω =1.5; (b) ω =2.0; and (c) ω =2.5

In this study, however, the phase trajectories and Poincaré map will be extensively used to investigate the dynamic behavior of the submerged payload. A phase trajectory is a geometric representation of the trajectories of a dynamical system in the phase plane. In other words, the phase trajectory plots the displacement versus the velocity of a system for a certain duration of time considered. For periodic solutions, a closed trajectory will be generated in the phase plane and for harmonic motions this closed trajectory will be exactly repeated after each period and will exactly overlapped the previous trajectory loop. Moreover, linear motions will create a circular closed trajectory while the nonlinearity will distort the trajectory shape. The Poincaré map, on the other hand, is a standard technique in dealing with the three dimensional phase space $(x, \dot{x}, t)$ of a periodically driven system and is used to inspect the projections $(x, \dot{x})$ whenever t is a multiple of $T = 2\pi/\omega$. Here, T is the periodic time of the forcing. It projects a two dimensional space $(x, \dot{x})$ onto a plane at a particular phase $\phi = \psi$, where ψ is a constant within [0, T]. Thus, the Poincaré map is a point set determined by the displacement $x_{\phi=\psi}$ and velocity $\dot{x}_{\phi=\psi}$ in a section corresponding to a given constant phase $\phi = \psi$. It should be mentioned that for the analysis presented in this paper the Poincaré map is generated at the phase $\phi = 0.7T$ in all cases. For a harmonic motion (defined as Period 1 motion), the Poincaré map will contain a single point, whereas, for a sub-harmonic motion of order n (defined as Period n motion) there will be n number of points in the Poincaré map. In the case of chaotic motion, the map has a complex fractal structure. More information regarding these analysis tools can be found in Thompson and Stewart (2002).

Fig. 4. Phase trajectories of payload pendulum motion for different wave maker motion frequencies at a = 0.01 and L_c = 0.5d [Cylinder Only]: (a) ω =1.5; (b) ω =2.0; and (c) ω =2.5

Fig. 5. Poincaré map of payload pendulum motion for different wave maker motion frequencies at a = 0.01 and L_c = 0.5d [Cylinder Only]: (a) ω =1.5; (b) ω =2.0; and (c) ω =2.5

Now, Fig. 4 and Fig. 5 show the resulting phase trajectories and Poincaré map for the Cylinder Only scenario under various frequencies of wave maker motion. As noticed, a stable sub-harmonic motion of order 5 can be identified for all the three frequencies considered. The existence of sub-harmonic motion can be visualized from the phase trajectories as well. A single trajectory loop is supposed to exist if no sub-harmonic motion is present. However, in this case it can be seen that the trajectories for various time periods are not exactly overlapping to create a single loop, but intersecting each other; and with the increase of wave frequency the intersection gaps are increasing, indicating that higher wave frequencies lead to stronger nonlinear motions.

Fig. 6. Comparisons of payload pendulum motion for different wave maker motion frequencies at a = 0.01 and L_c = 0.5d [Beam Sea Up]: row 1: time history of motion; row 2: phase trajectories; and row 3: Poincaré map

Following the similar approach, the Poincaré map and phase trajectories for rest of the three orientations (Beam Sea Up, Beam Sea Dn and Head Sea) are plotted and shown in Fig. 6 to Fig. 8. The most significant impact generated by the presence of the barge in these three orientations, compared to the previous 'Cylinder Only' case, is the introduction of frequency doubling, period doubling and possible chaotic behavior in the responses of submerged payload. For example, Fig. 6 illustrates that for the Beam Sea Up case, a period-20 motion is observed at ω = 1.5 and a period-10 motion is observed at ω = 2. That means a frequency doubling phenomenon must exist between frequencies of 1.5 to 2.0. As the frequency increases a period-25 motion is observed at ω = 2.5, leading towards the possible chaotic behavior of the payload. The phase trajectories also confirm that increase of frequency is leading towards stronger nonlinearity in payload motions, thus producing more complex overlapping in the phase plane.

Fig. 7. Comparisons of payload pendulum motion for different wave maker motion frequencies at a = 0.01 and L_c = 0.5d [Beam Sea Dn]: row 1: time history of motion; row 2: phase trajectories; and row 3: Poincaré map

Fig. 8. Comparisons of payload pendulum motion for different wave maker motion frequencies at a = 0.01 and L_c = 0.5d [Head Sea]: row 1: time history of motion; row 2: phase trajectories; and row 3: Poincaré map

For the Beam Sea Dn scenario, on the other hand, the amplitude of payload motion seems to reduce significantly, which is reasonable (Fig. 7), because in this orientation the payload is shielded by the presence of the crane barge in the upstream side. Therefore the payload is not receiving the direct impact of the generated waves. However, a period doubling in payload motions occurs between the frequencies of 1.5 to 2.0. Also, the phase trajectories of the payload are found to differ significantly for the frequencies of 2.0 and above compared to all other scenarios. The payload at these frequencies appears to undergo considerable transient motions before reaching the periodic form.

Finally, Fig. 8 represents the results for the Head Sea scenario which is the closest case to the Cylinder Only scenario, from the geometric orientation point of view. However, unlike the cylinder only case (Fig. 5) the payload here faces a period doubling between ω = 1.5 to 2.0. Also, with the increase of wave frequency the influence of low frequency components in the payload motion appears to be stronger compared to those plotted in Fig. 3 for Cylinder Only. The phase trajectory for these two scenarios starts to differ considerably as the frequency rises. Especially, at $\omega = 2.5$ the payload at the Head Sea orientation observes a transient motion while such motion cannot be found for the Cylinder Only case.

3.2 Bifurcation and spectral analysis

In a dynamical systems (similar to the problem considered in this study), a bifurcation occurs when a small change made to the parameter values (the bifurcation parameters) of a system causes a sudden qualitative or topological change in its behavior. Bifurcation analysis is therefore, widely applied to to investigate the stability of system behavior, using point sets in a Poincaré map, as the control parameter is changed. The corresponding Bifurcation diagram illustrates how the equilibrium state (point set in Poincaré map or impact map) changes while a control parameter is gradually increased (Lee 2005). Fig. 9 shows such Bifurcation diagrams for the various geometric configuration considered in this study. Here, the wave frequency is set as the control parameter and the displacements of all the points in the Poincaré map are plotted against the corresponding frequencies (for $\omega = 1.5$ to 2.5, at an interval of 0.1).

Fig. 9. Bifurcation diagram for varying wave frequencies at $a = 0.01$ and $L_c = 0.5d$: (a) Cylinder Only; (b) Head Sea; (c) Beam Sea Up; and (d) Beam Sea Dn

As depicted, the period doubling phenomena in Head Sea and Beam Sea Dn are clearly distinguishable (the number of points for $\omega = 1.6$ becomes double compared to that of $\omega = 1.5$). Whereas, in Beam Sea Up the motion experiences frequency doubling, leading towards quasi-periodic motion and then followed by period doubling as the frequency rises. Also, the range for point sets in the Poincaré map varies quite noticeably for all the cases, especially for those where the floating barge is placed near the submerged payload, suggesting the influence of high nonlinearity. For the cylinder only scenarios, a consistent period-5 motion is observed irrespective of the change of frequency. After the period doubling occurs (at $\omega = 1.6$), the Head Sea orientation also exhibits a stable sub-harmonic motion afterwards as the frequency continues to increase. Nevertheless, the motions appear to spread over a broader band at higher frequencies, indicating the presence of transient motions.

The Beam Sea Up and Beam Sea Dn on the other hand, are found to exhibit possible quasi-periodic response at ω = 1.8 and ω = 2.3 respectively. Quasi-periodicity is the property of a system that displays irregular periodicity. Periodic behavior is defined as recurring at regular intervals, whereas, quasi-periodic behavior is a pattern of recurrence with a component of unpredictability that makes the motion recurring at irregular intervals. To further investigate the possible reason behind these quasi-periodic motions, frequency spectra for these two scenarios are examined in Fig. 10 in order to identify the influence of forcing, natural frequency and harmonic on nonlinear interactions. The amplitudes are plotted both in linear and log scales for clear depiction of the nonlinearity in the responses.

Fig. 10. Frequency spectra for the motion of the cylinder at a = 0.01 and L_c = 0.5d: Beam Sea Up (ω=1.8) [(a) Linear scale; (b) Logarithmic scale]; and Beam Sea Dn (ω=2.3) [(c) Linear scale; (d) Logarithmic scale]

As can be seen, the peak at 1ω is the response at the forcing frequency and a small 2nd harmonic is also observed (other higher harmonics are negligible, therefore not shown here). Careful observation of log scale plots also reveal a broad band of small peaks covering many frequencies (especially between 0 to 1.5 ranges), instead of usual one or two sharp peaks. This is an indication of the existence of quasi-periodic motion. However, the most interesting behavior is the presence of low frequency peaks near 0.1ω and 0.2ω for Beam Sea Up and near 0.2ω for Beam Sea Dn. According to Hannan and Bai (2015), the natural frequency of the submerged payload for the particular cable length studied here is 0.384; which after normalizing becomes: ω_0 / ω_{wave} = 0.384/2.0 = 0.192 ≈0.20. Therefore, it can be said that the quasi-periodic motion of the payload here is highly influenced by its natural frequency. The low frequency components are mostly excited due to the effect of nonlinearities from shielding, as well as due to the effect of the natural frequency.

At this point, it might also be worthwhile to investigate quantitatively that how the effect of nonlinearity is changing over the range of frequency changes for the rest of the scenarios. In order to do so, the various components of payload motion (mean, low frequency harmonics, linear 1st order as well as higher harmonics) obtained from the FFT analysis are plotted in Fig. 11 with respect to the normalized wave frequency kr, where $k = 2\pi / \lambda$, is the wave number. Here, all the components are plotted as a percentage of total motion amplitude of the payload. The 'mean' is the mean zero frequency component of the motion amplitude. 'Low freq' is the summation of first two low frequency harmonics. The low frequency harmonics are found to appear as harmonics of 0.1ω (Hannan and Bai 2015) and mostly the 0.1ω and $0.2\omega^{th}$ components contributes significantly towards the total response. '1^{st} Order' represents the forcing frequency component. The rest of the components (including higher order harmonics) are summed up and considered inside the term 'others' as shown in the figure.

Fig. 11. Pendulum motion amplitude of the payload as percentages of various components with the variation of wave frequency at a = 0.01 and L_c = 0.5d: (a) Cylinder Only; (b) Head Sea; (c) Beam Sea Up; and (d) Beam Sea Dn

Now, as can be seen in Fig. 11, around 70-95% of payload motion amplitudes at lower wave motion frequency come from linear response. Because, the wave length at this lower frequency range of wave maker is quite large compare to the size of the barge and payload. Thus, not much shielding or nonlinear effects are involved. However, as the wave frequency increases the percentage of nonlinear low frequency components and 'mean' start to rise significantly for all the various geometric configurations presented in this study. For the beam sea upstream case, the mean appears to reach as much as 55%. The beam sea downstream cases on the other hand, are found to experience fairly 'low frequency component' dominated motion which is around 70% of total motion amplitude for kr values above 0.6.

Therefore, it can be concluded that change of wave frequency coupled with various orientations of the floating barge and submerged payload significantly alters the payload motion behaviour and introduces various nonlinear phenomena. For different orientations, the effects of changing wave frequencies seem to follow different trends.

4. Variation in payload pendulum motion dynamics for different cable lengths

Initial length of the cable from which the submerged payload is hanging is one of the most important controlling parameters for the operation of offshore crane barge. This section studies the variation of payload response with respect to the change of this cable length. In order to change the length of cable, the rotation point of the cable (crane tip) is shifted accordingly instead of moving the cylinder under water. This means the initial under water position of the cylinder remains unchanged, which is 0.2d below the undisturbed free surface.

Moreover, the motion amplitude and frequency of the wave are also kept constant. Fig. 12 helps to clarify this scenario.

Fig. 12. Sketch representing the change of cable length scenarios

In reality, shifting the crane tip might not be a consistent option. However, the reason behind such selection here is that: during the installation process, one of the major challenges is to lower the payload through the 'splash zone' as most of the severe wave interactions will happen in this region. Hence, the payload here is kept near this free surface zone and investigation is performed to understand whether an initial long or short length of the cable is better to start the installation process. In addition, maintaining the same underwater position of the payload for various cases will help to make comparison among the cases in a much meaningful way.

Fig. 13. Phase trajectories of payload motion for various cable lengths at a = 0.015 and ω = 2.0: row 1: Cylinder Only; row 2: Head Sea; row 3: Beam Sea Up; and row 4: Beam Sea Dn

Fig. 13 presents the comparison of phase trajectories among the four different geometric orientations of the payload and crane barge under the influence of three different cable lengths. Here, the horizontal component of the pendulum motion of the payload is plotted instead of the angular motion in order to ensure a proper non-dimensionalized comparison. As can be seen, for the cylinder only case, the change of cable length does not produce any significant impacts. The similar conclusion can be drawn for the other three scenarios as well, except slight increases in the displacement with the increase of cable length. Besides, as already discussed in the previous section, the phase trajectories for the Beam Sea Dn case are easily distinguishable from the rest of the scenarios indicating the influence of significant shielding effect generated by the presence of floating barge in the upstream side of the flow. In fact, the nonlinearities in phase trajectories due to the shielding effect can be visualized in the Head Sea and Beam Sea Up cases as well, compared to the phase trajectories of Cylinder Only case, although the influences are not quite prominent as the Beam Sea Up case.

Fig. 14. Influence of cable length on dynamics of phase motions at a = 0.015 and ω = 2.0: (a) Cylinder Only; (b) Head Sea; (c) Beam Sea Up; and (d) Beam Sea Dn

Fig. 14 plots the changes in the point set of the Poincaré map as the cable length is gradually increased. As noticed and already concluded, change of cable length only produces limited additional nonlinear impact on payload motions. Points in the Poincaré map appear to spread over similar ranges for all the cable lengths under a certain orientation, except the Beam Sea Up case. At this particular frequency of 2.0, the hydrodynamic properties of the floating barge in the Beam Sea Up orientation are found to significantly influence the underwater motion of the payload (Hannan and Bai 2015) as the length of the crane barge in this situation nearly coincides with the incoming wave length; consequently, resulting a large mean drift motion of the payload. This large mean drift force keeps increasing with the increase of cable length as seen in Fig. 14(c).

Fig. 15. Pendulum motion amplitude of the payload as percentages of various components with the variation of cable length at a = 0.015 and ω = 2.0: (a) Cylinder Only; (b) Head Sea; (c) Beam Sea Up; and (d) Beam Sea Dn

Fig. 15 will help to visualize these effects of nonlinearity in a more concise way. Here, the various components of payload's motion obtained via FFT are plotted as a percentage of total motion amplitude. As can be seen in this figure and already mentioned for Fig. 14, the percentage of mean drift in total motion amplitude increases with the increase of cable length for the beam sea upstream cases. Whereas for the single cylinder and head sea cases, the contribution from low frequency harmonics seems to increase more noticeably compared to the mean drift and for head sea cases the contribution exceeds 60 % at largest cable length considered. The beam sea downstream cases on the other hand, always governed by the low frequency harmonic responses. Though, the influence of mean drift motion also becomes noticeable with the increase of cable length.

Fig. 16. Ranges (maximum to minimum) of mean and low frequency components of payload motions for cable length changes under various geometric configurations at a = 0.015 and ω = 2.0.

Finally, Fig. 16 of this subsection illustrates the actual nondimensionalized ranges over which the mean drift motion and low frequency components of the payload motion varies with the change of cable length. The range for mean drift motion of beam sea up cases is between 5.63 to 6.77 which is fairly big compared to the ranges of other scenarios. Thus, it is not shown in this figure for better comparability of mean drift motion of other scenarios. Now, as depicted, the ranges for both the mean and low frequency components varies quite significantly in terms of span as well as position, for various geometric orientation of the barge and payload. These variations cannot be captured from the earlier Fig. 15. As seen, the mean drift motion for head sea cases varies over a long range for the various cable lengths considered, compared to the cylinder only and beam sea Dn scenarios. Similarly, the low frequency contributions for the beam sea Dn cases varies over the longest range among all the four scenarios, although, in percentage wise the contribution for all the cases looks similar as shown in Fig. 15. The least influence of lower harmonics is found for the cylinder only cases, which is reasonable as there is no shielding effect here. Therefore, it can be said that the global impact of nonlinearity in payload's motion with the change of cable length is less prominent compared to its influence with the change of wave motion frequency. However, change of cable length can still generate noticeable variations among the responses of the payload under different geometric orientation.

5. Nonlinear dynamics of payload moving downwards

The previous sections investigated the nonlinear dynamics involved in pendulum motions of the payload under various scenarios while no vertical motion of the crane tip is allowed. This section considers a more practical approach; besides the constrained pendulum motion, the payload here is allowed to have a constant downward motion as if the crane vessel is lowering it down towards the sea bed. The payload in this case therefore, subjected to the coupled influence of wave action and downward motion of the rigid cable to which it is attached. Among the four different arrangements considered in the previous sections, the Cylinder Only and Head Sea configurations are investigated here. A comparatively longer cable length ($L_c = 0.8d$) is chosen to study the present situation, and the cylinder in this case is initially placed at $0.15d$ below the undisturbed free surface. The downward motion of the payload is denoted by V_d in this study and its unit is set as distance travelled per wave period instead of distance travelled per second. Also, at the beginning of the simulation, 5.5 wave periods are allowed as an initial build up time to ensure that the fully generated wave reaches the submerged payload and floating barge arrangement. The cylinder is allowed to move downward after this initial period is over.

5.1 Variation of wave frequencies

At first the behaviour of the payload moving towards the sea bed is investigated under different frequencies of the wave motion while the motion amplitude of the wave maker and downward moving speed of the cylinder are kept constant at 0.015 and 0.02 respectively. Fig. 17 shows the corresponding phase trajectories and Poincaré map for the Head Sea case plotted for the 10-20 time periods.

Fig. 17. Influence of wave frequency variation on the dynamics of moving downward payload at $V_d = 0.02d$, $a = 0.015$ [Head Sea]: row 1: phase trajectories; and row 2: Poincaré map

As can be seen from the phase trajectories, more complex overlaps occur in the phase plane as the wave frequency rises, indicating that the nonlinearity increases in the payload motion at the same time. This increase in nonlinearity can be related to the low frequency components inside the payload motion. However, unlike Section 3 where the period doubling and frequency doubling phenomena were observed with the increase of frequency, a stable period-10 motion is only identified here in the payload motion irrespective of various frequencies. This can be explained as follows: in Section 3, the payload is not allowed to have any downward motion thus exposing it to all sorts of near surface nonlinear phenomena for the entire simulation period. Whereas in this case, the payload is constantly going towards the sea bed, thus the influence of strong nonlinearities is decreasing as it is moving away from the free surface zone.

5.2 Influence of moving downward speed

Several cases have been simulated in this subsection for both the Cylinder Only and Head Sea configurations considering different downward speeds of the payload motion, keeping the wave maker motion amplitude constant at 0.015. Fig. 18 illustrates the phase trajectories for four different V_d in the Head Sea condition. All these trajectories appear to be in similar shapes except that the range of payload motion decreases with the increase of V_d. This is reasonable in the physical sense, because the increase of V_d means the payload is moving towards the sea bed at a faster speed, therefore, getting lesser attention of the free surface wave and other associated disturbance and resulting the smaller motion amplitude of the payload. The similar shapes for the trajectories, on the other hand, indicate that variation of V_d does not create significant additional nonlinearities other than what already exists in the payload motion.

Fig. 18. Variation in the phase trajectories of the payloads due to various moving downwards speeds at $L_c = 0.8d$, $\omega = 2.0$, $a = 0.015$ [Head Sea]: (a) $V_d = 0.005$; (b) $V_d = 0.01$; (c) $V_d = 0.015$; and (d) $V_d = 0.02$

Fig. 19 compares the Poincaré maps between the Cylinder Only and Head Sea scenarios under the influence of various V_d. As can be seen, all the cases undergo a period-10 motion and the point sets in the Poincaré map for all the cases appear to follow a similar pattern irrespective of V_d, thus confirming the conclusion of Fig. 18. However, the range for the point sets of the Head Sea case appears to be much longer than that of the Cylinder Only case. The presence of floating barge in the Head Sea case produces stronger nonlinear effects in the payload motion, even when the payload is moving towards the sea bed.

Fig. 19. Comparison of Poincaré map between the Cylinder only and Head Sea orientations of the moving downwards payload under various moving downwards speeds with $L_c = 0.8d$, $\omega = 2.0$, $a = 0.015$: (a) $V_d = 0.005$; (b) $V_d = 0.01$; (c) $V_d = 0.015$; and (d) $V_d = 0.02$

5.3 Payload moving downwards under various motion amplitudes of wave

The final subsection of this paper investigates the influence of the motion amplitude of the wave on the dynamic response of the payload while it moves with a constant downward velocity of $V_d = 0.02d$. Fig. 20 depicts the corresponding phase trajectories and Poincaré map obtained for the Head Sea case with various motion amplitudes of the wave maker.

Fig. 20. Influence of various motion amplitudes of wave maker on dynamic behavior of payload moving downwards with L_c = 0.8d, ω = 2.0 [Head Sea]: column 1: phase trajectories; column 2: Poincaré map; row 1: a = 0.005; row 2: a = 0.01; row 3: a = 0.015; and row 4: a = 0.02

Irrespective of the increase of wave maker motion amplitude, the payload appears to face a period-10 motion. The phase trajectories show that the amplitude of motion increases as the wave maker motion amplitude increases. From the increasingly complex overlapping of the phase loops it can also be said that the nonlinearity in payload motion increases at the same time. Besides, with the increase of wave maker motion amplitude, the presence of low frequency component with transient motion can be found as well, especially at a = 0.02.

Overall, it is identified that the change of moving downward speed of the payload does not produce any significant influence towards the nonlinear motion of the payload after the payload reaches a certain depth from the free surface, whereas, the increase of incoming waves amplitude or frequency still may noticeably increase the nonlinearity of payload motion.

Fig. 21. Wave profile snapshots at t =9.5T with a = 0.02, ω = 2.0: (a) Head sea; (b) Beam Sea Up; and (c) Beam Sea Dn

Finally to provide a visual impression of the simulation output, three snapshots of free surface profiles captured at a particular time instant of the simulation period are presented in Fig.21. The snapshots are captured after the simulation reaches a fully developed state. The waves here are propagating from the left end of the tank and the damping layer is situated at the far right end side. The effectiveness of the damping layer is quite evident from these pictures as the wave elevation is almost zero at the layer zone. It is also noticed that the presence of submerged cylinder near the barge in the Head Sea creates noticeable disturbance on free surface compared to the other side of the barge (Fig. 21(a)). Moreover, the interactions between the incoming wave from the wave maker and diffracted wave from the barge wall in both the Beam Sea cases are also visible in Fig. 21(b) and Fig. 21(c). These two figures also clearly reveal the influence of submerged cylinder on wave profile as well as on barge run-up when the cylinder is in the upstream side (Fig. 21(c)).

6. Conclusions

The nonlinear dynamics of fully submerged payload of offshore crane barge is investigated numerically. An established fully nonlinear time domain model is applied to solve the problem. The computation is carried out for the coupled system of a fixed crane barge and a fully submerged payload subjected to constrained pendulum motions. Analysis tools such as the Poincaré map, bifurcation diagram, and phase trajectories are used to analyse the results. The periodicity of the nonlinear motion is being traced effectively using the Poincaré map. The effects of changing wave frequency on the motion characteristics have been well demonstrated and it is found that nonlinearities have a significant influence on the dynamics of the submerged payload movement, especially at a certain range of wave frequencies. Besides, the existences of various nonlinear phenomena, for example the sub-harmonic motions of Period-5, Period-10 and Period-20 and period doublings are captured. The results also indicate that different orientations of the floating barge and submerged payload system are responsible for the different dynamic behaviour of the payload. The presence of nearby floating barge, even when the payload is moving downwards, introduces noticeable nonlinearity in payload motion.

It should be recalled, however, that further research is needed to extend the present model in order to achieve improved understanding of this problem. The effect of the motion of floating barge along with mooring lines will be considered in the future study, which is known as another source of significant nonlinear behaviour.

References

Bai, W., and Eatock Taylor, R. (2006). "Higher-order boundary element simulation of fully nonlinear wave radiation by oscillating vertical cylinders." *Appl. Ocean Res.*, **28**(4), 247-265.

Bai, W., Hannan, M. A., and Ang, K. K. (2014). "Numerical simulation of fully nonlinear wave interaction with submerged structures: fixed or subjected to constrained motion." *J. Fluids Struct.*, **49**, 534-553.

Balachandran, B., Li, Y. Y., and Fang, C. C. (1999). "A mechanical filter concept for control of non-linear crane-load oscillations." *J. Sound Vib.*, **228**, 651-682.

Cha, J.-H., Roh, M.-I., and Lee, K.-Y. (2010). "Dynamic response simulation of a heavy cargo suspended by a floating crane based on multibody system dynamics." *Ocean Eng.*, **37**, 1273-1291.

Chen, M., Eatock Taylor, R., and Choo, Y. S. (2014). "Time domain modeling of a dynamic impact oscillator under wave excitations." *Ocean Eng.*, **76**, 40-51.

Clauss, G., and Riekert, T. (1989). "Studies of the operating limits of crane ships in wave groups (Untersuchungen der Einsatzgrenzen von Kranschiffen in Wellengruppen)." *Entwicklung in der Schiffstechnik (Statusseminar) [Development in marine technology (Status Conference)]*, Germanischer Lloyd Hamburg, 106-131.

Clauss, G., and Riekert, T. (1990). "Operational limitations of offshore crane vessels." *Proc. of OTC*, Houston, TX, OTC 6217, 161-170.

Clauss, G., and Riekert, T. (1992). "Influence of load motion control on the operational limitations of large crane vessels in severe environment." *Proc. Int. Conf. on Behaviour of Offshore Structures*, London, 1112-1125.

Clauss, G. F., and Vannahme, M. (1999). "An experimental study of the nonlinear dynamics of floating cranes." *Proc. of 9th ISOPE*, Fance, 511-518.

Ellermann, K. (2005). "Dynamics of a moored barge under periodic and randomly disturbed excitation." *Ocean Eng.*, **32**(11-12), 1420-1430.

Ellermann, K., and Kreuzer, E. (1999). "Nonlinear Dynamics in Crane Ship Motion." *Proc. of 3rd European Nonlinear Oscillations Conference*, Technical University of Denmark, DK-2800 Lyngby, Denmark.

Ellermann, K., and Kreuzer, E. (2003). "Nonlinear dynamics in the motion of floating cranes." *Multibody Sys.Dyn.*, **9**, 377-387.

Ellermann, K., Kreuzer, E., and Markiewicz, M. (2002). "Nonlinear dynamics of floating cranes." *Nonlinear Dyn.*, **27**, 107-183.

Gavassoni, E., Batista Gonçalves, P., and de Mesquita Roehl, D. (2015). "Nonlinear vibration modes of an offshore articulated tower." *Ocean Eng.*, **109**, 226-242.

Hannan, M. A., and Bai, W. (2015). "Nonlinear hydrodynamic responses of submerged moving payload in vicinity of a crane barge in waves." *Mar. struct.*, **41**, 154-179.

Hassan, A. M. A., Downie, M. J., Incecik, A., whelan, J., and Graham, J. M. R. (2010). "Wave drift forces and responses in deep water and extreme environmental conditions." *HYDRALAB III Joint User Meeting*, Hannover, Germany.

Jiang, T. (1991). Investigation of nonlinear ship dynamics involving instability and chaos in examples from offshore technology. PhD, Institute of Shipbuilding of the University of Hamburg.

Lee, J. Y. (2005). "Motion behavior of impact oscillator." *J. Mar. Sci. Appl.*, **12**(2), 89-96.

Liaw, C. Y. (1988). "Bifurcations of subharmonics and chaotic motions of articulated towers." *Eng. Struct.*, **10**(2), 117-124.

Liaw, C. Y., Shankar, N. J., and Chua, K. S. (1992). "Subharmonic moitons and wave force-structure interaction." *Mar. struct.*, **5**, 281-295.

Lin, H., and Yim, S. C. S. (1995). "Chaotic roll motion and capsize of ships under periodic excitation with random noise." *Appl. Ocean Res.*, **17**(3), 185-204.

McCormick, F., and Witz, J. (1993). "An investigation into the parameter excitation of suspended loads during crane vessel operations." *Underwater Technology*, **19**, 30-39.

Patel, M., Brown, D., and Witz, J. (1987). "Operability analysis for a monohull crane vessel." *Transactions of the Royal Institution of Naval Architects*, **129**, 103-113.

Raghthama, A., and Narayanan, S. (2000). "Bifurcation and chaos of an articulated loading platform with piecewise non-linear stiffness using the incremental harmonic balance method." *Ocean Eng.*, **27**(10), 1087-1107.

Sarkar, A., and Eatock Taylor, R. (1998). "Low frequency responses of non linearly moored vessels in random waves: development of a two scale perturbation method." *Appl. Ocean Res.*, **20**, 225-236.

Thompson, J. M. T., and Stewart, H. B. (2002). *Nonlinear Dynamics and Chaos*, John Wiley & Sons Inc.

Witz, J. A. (1995). "Parametric excitation of crane loads in moderate sea states." *Ocean Eng.*, **22**(4), 411-420.

Witz, J. A., Ablett, C. B., and Harrison, J. H. (1989). "Roll response of semisubmersibles with non-linear restoring moment characteristics." *Appl. Ocean Res.*, **11**(3), 153-166.

Yim, S. C. S., and Lin, H. (1991). "Chaotic behavior and stability of free-standing offshore equipment." *Ocean Eng.*, **18**(3), 225-250.

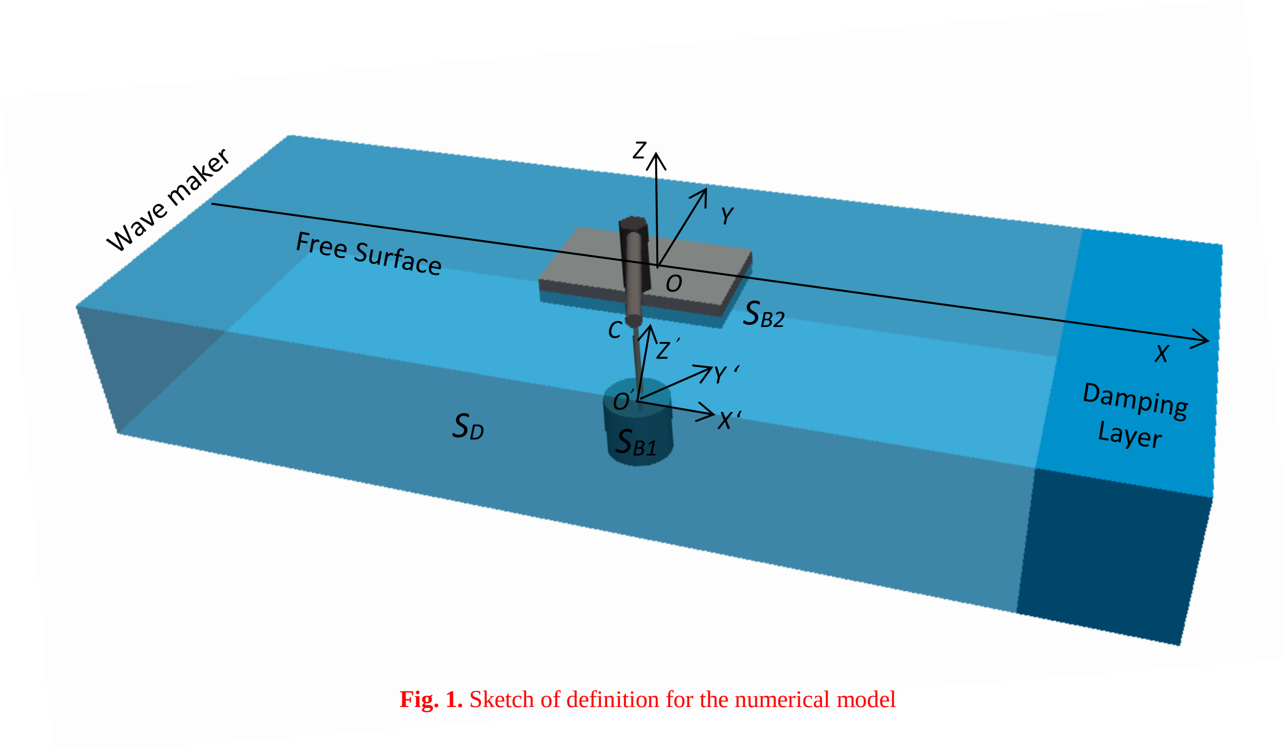

Fig. 1. Sketch of definition for the numerical model

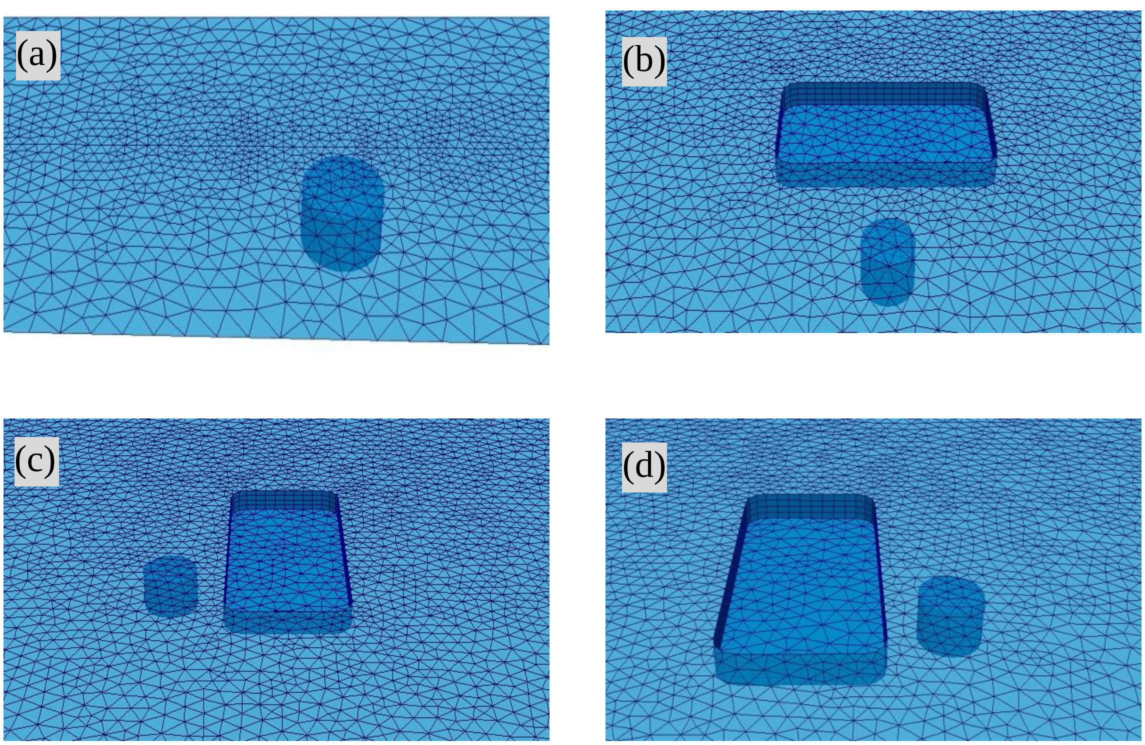

Fig. 2. Mesh generated for various configurations: (a) Cylinder Only; (b) Head Sea; (c) Beam Sea Up; and (d) Beam Sea Dn

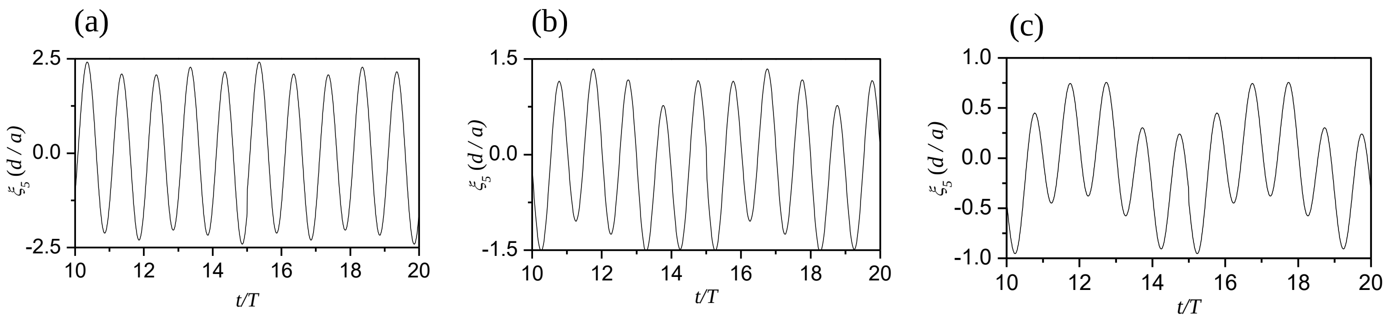

Fig. 3. Time histories of cylinder motion for different wave maker motion frequencies at a = 0.01 and L_c = 0.5d [Cylinder Only]: (a) ω =1.5; (b) ω =2.0; and (c) ω =2.5

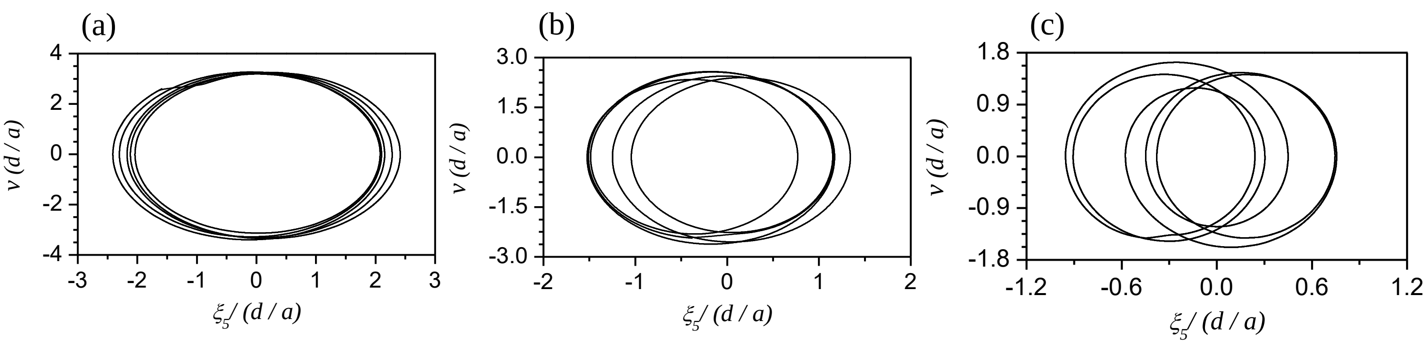

Fig. 4. Phase trajectories of payload pendulum motion for different wave maker motion frequencies at a = 0.01 and L_c = 0.5d [Cylinder Only]: (a) ω =1.5; (b) ω =2.0; and (c) ω =2.5

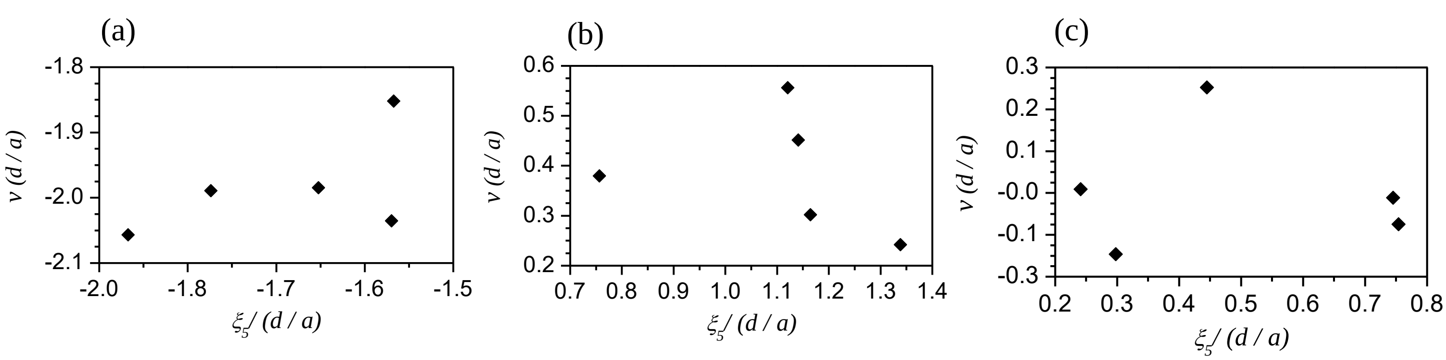

Fig. 5. Poincaré map of payload pendulum motion for different wave maker motion frequencies at a = 0.01 and L_c = 0.5d [Cylinder Only]: (a) ω =1.5; (b) ω =2.0; and (c) ω =2.5

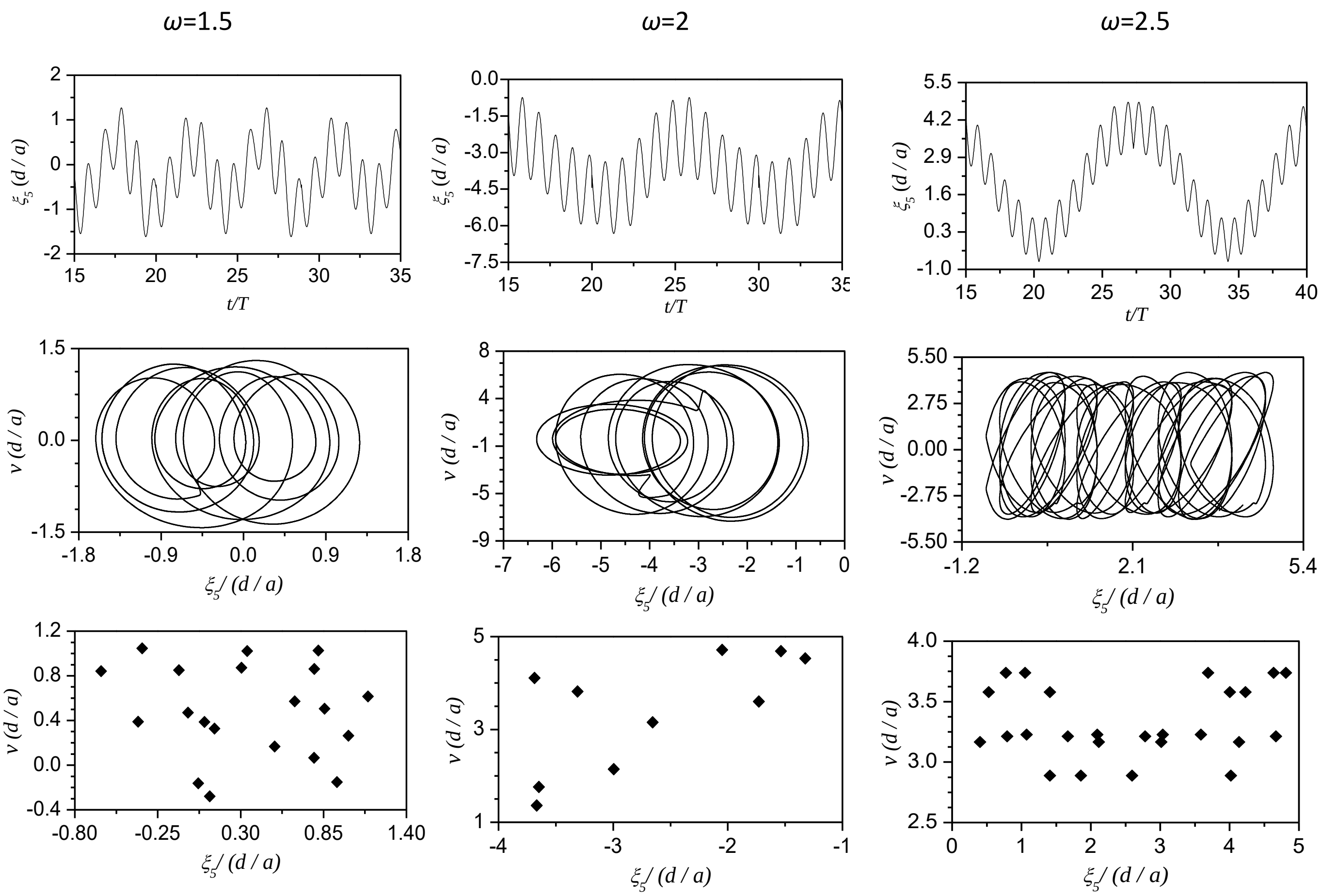

Fig. 6. Comparisons of payload pendulum motion for different wave maker motion frequencies at a = 0.01 and L_c = 0.5d [Beam Sea Up]: row 1: time history of motion; row 2: phase trajectories; and row 3: Poincaré map

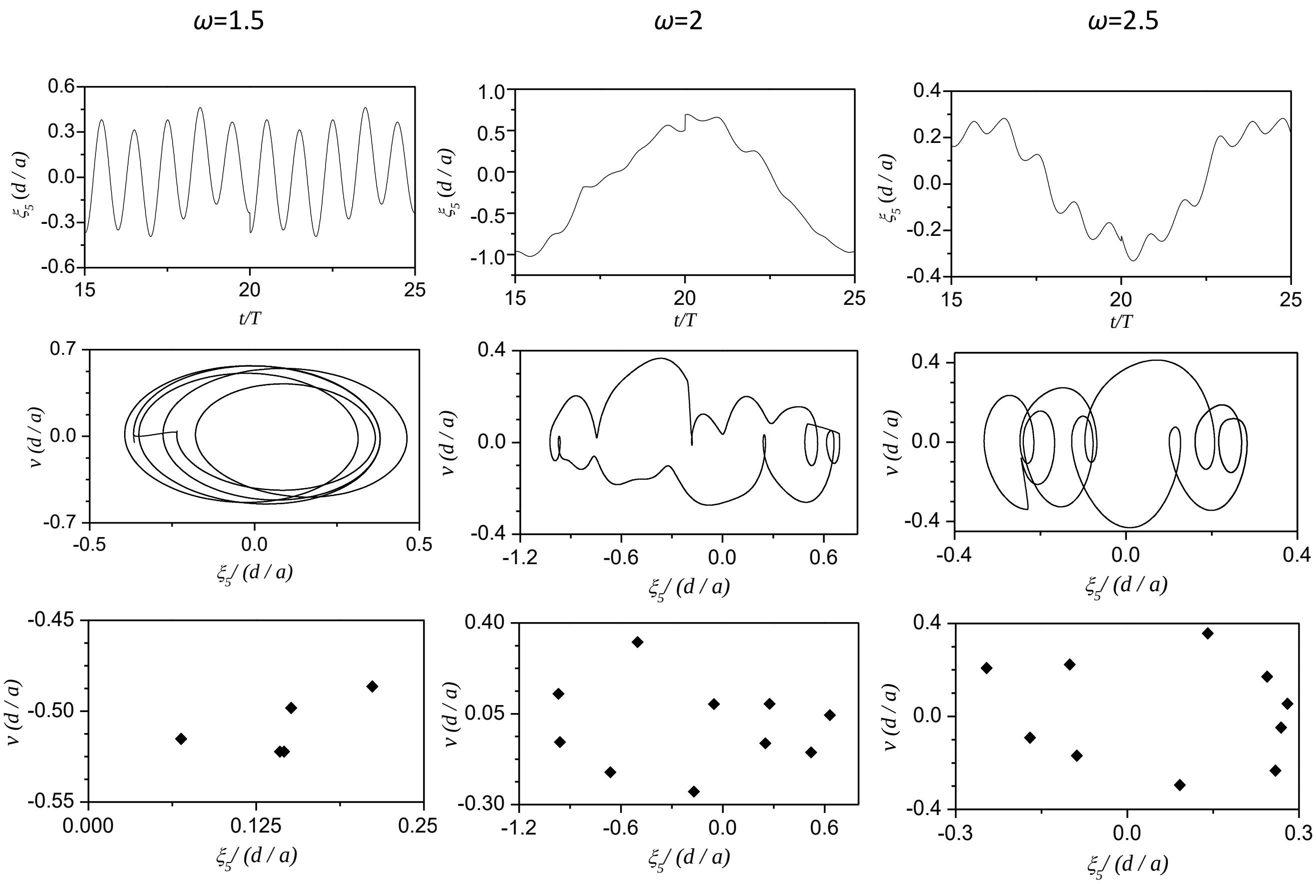

Fig. 7. Comparisons of payload pendulum motion for different wave maker motion frequencies at a = 0.01 and L_c = 0.5d [Beam Sea Dn]: row 1: time history of motion; row 2: phase trajectories; and row 3: Poincaré map

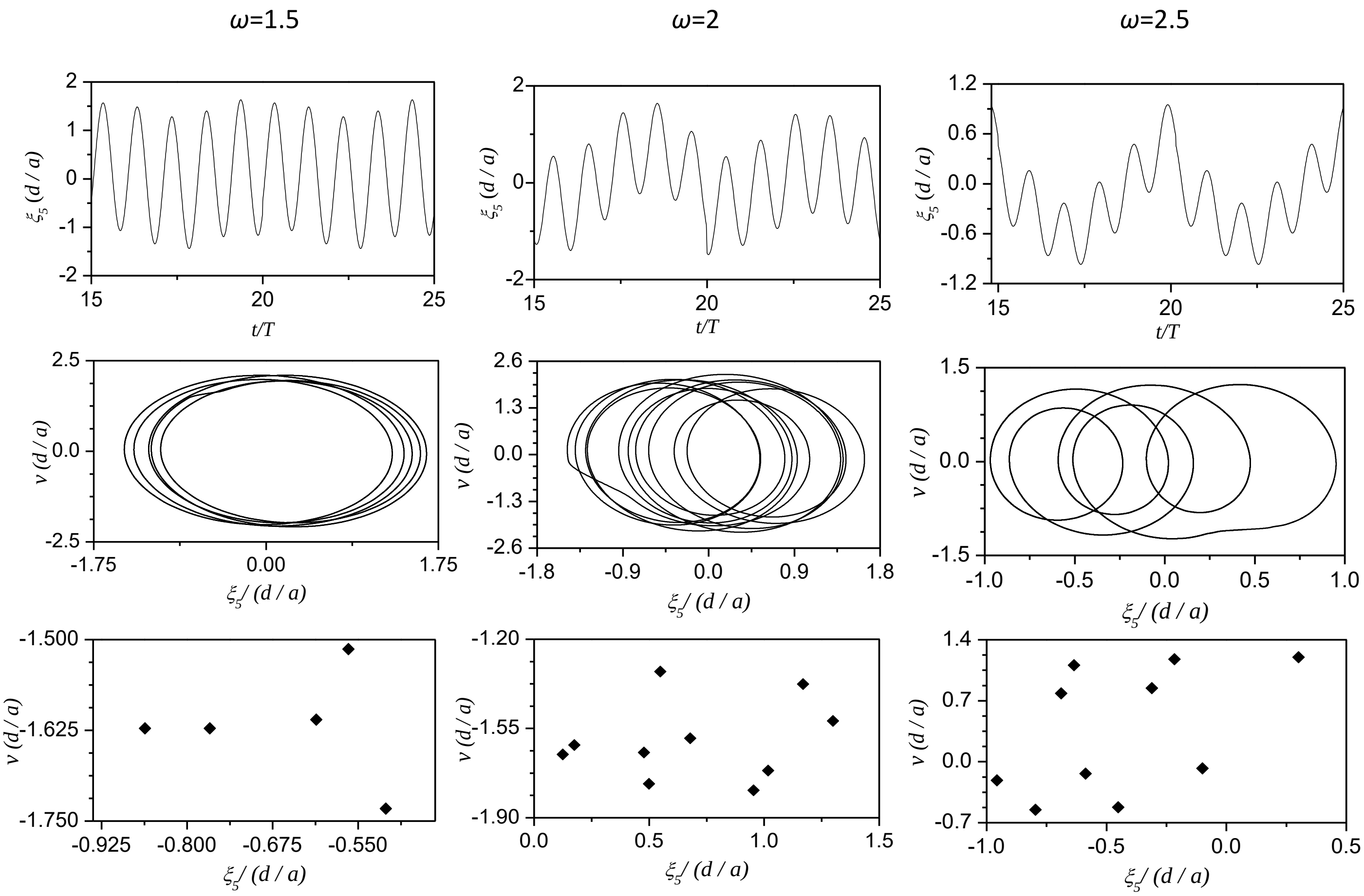

Fig. 8. Comparisons of payload pendulum motion for different wave maker motion frequencies at a = 0.01 and L_c = 0.5d [Head Sea]: row 1: time history of motion; row 2: phase trajectories; and row 3: Poincaré map

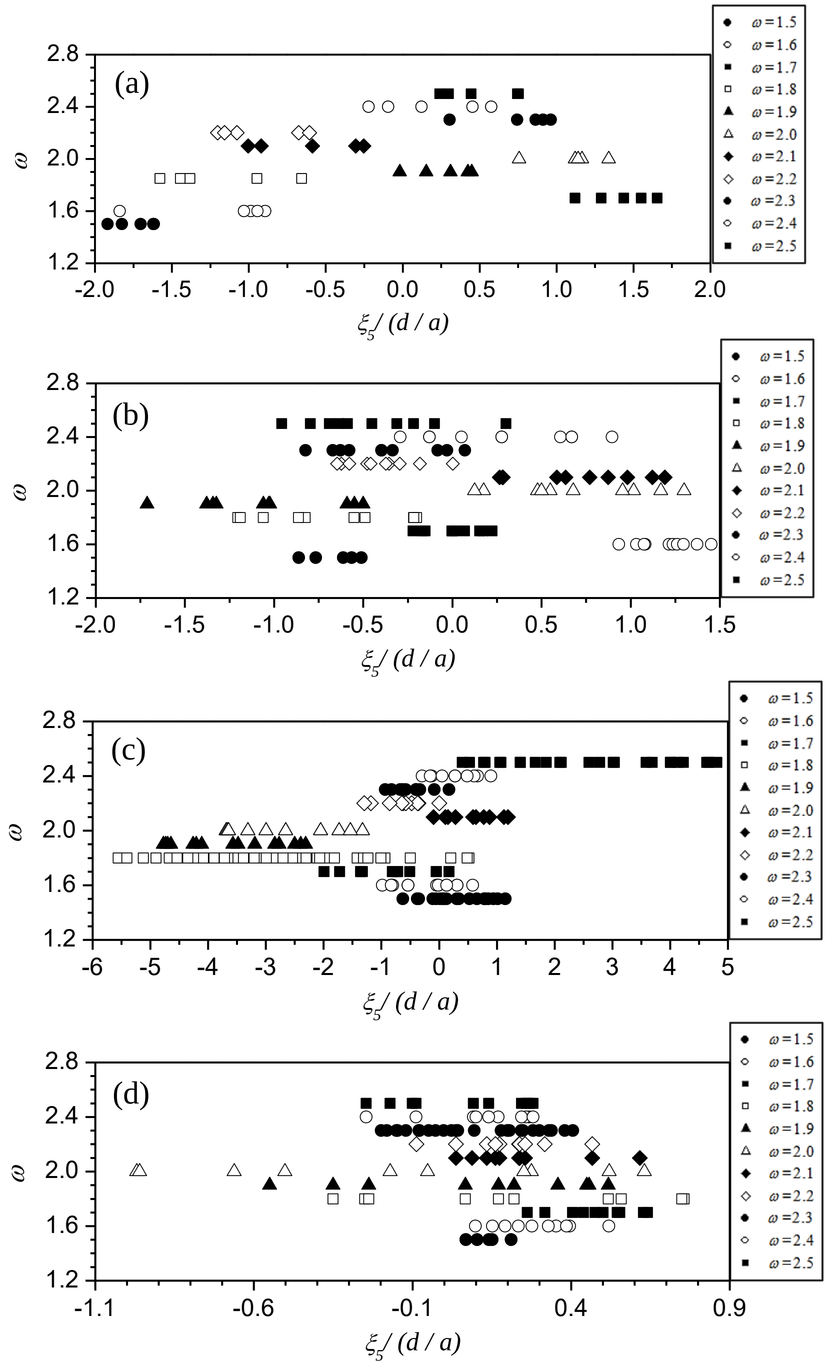

Fig. 9. Bifurcation diagram for varying wave frequencies at a = 0.01 and L_c = 0.5d: (a) Cylinder Only; (b) Head Sea; (c) Beam Sea Up; and (d) Beam Sea Dn

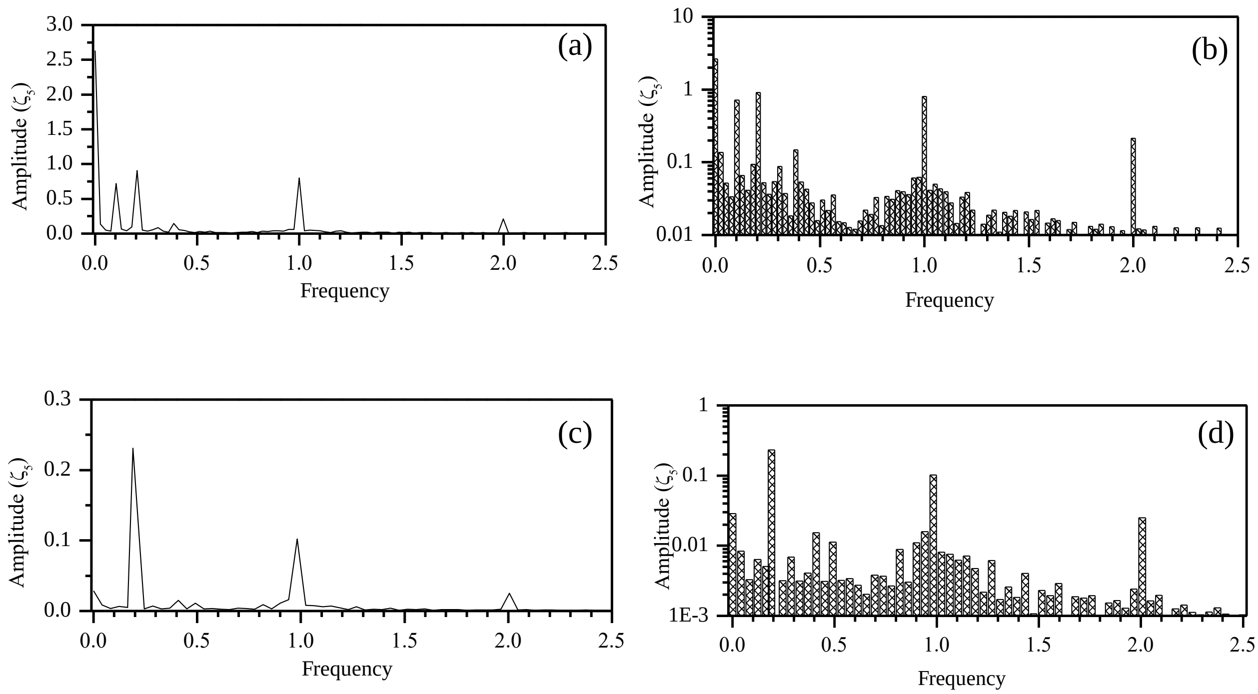

Fig. 10. Frequency spectra for the motion of the cylinder at a = 0.01 and L_c = 0.5d: Beam Sea Up (ω=1.8) [(a) Linear scale; (b) Logarithmic scale]; and Beam Sea Dn (ω=2.3) [(c) Linear scale; (d) Logarithmic scale]

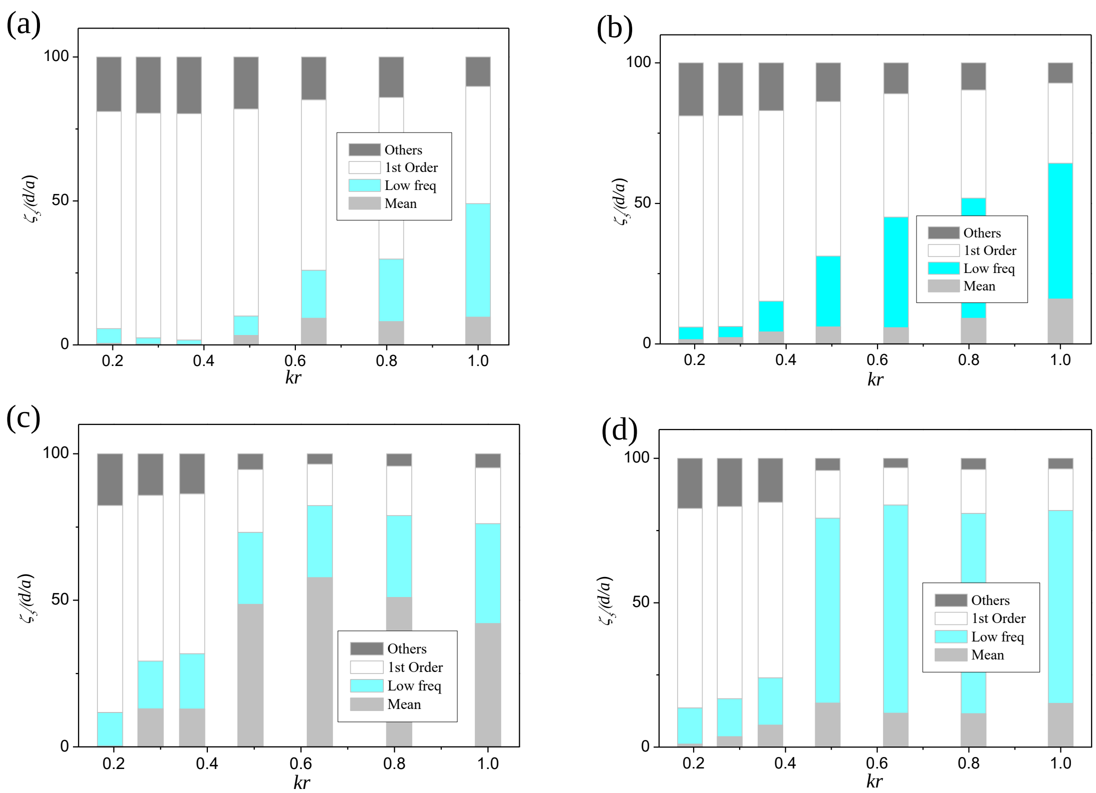

Fig. 11. Pendulum motion amplitude of the payload as percentages of various components with the variation of wave frequency at a = 0.01 and L_c = 0.5d: (a) Cylinder Only; (b) Head Sea; (c) Beam Sea Up; and (d) Beam Sea Dn

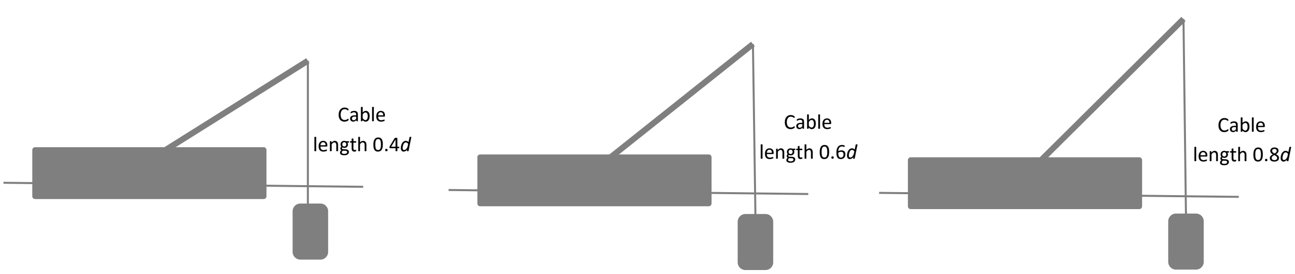

Fig. 12. Sketch representing the change of cable length scenarios

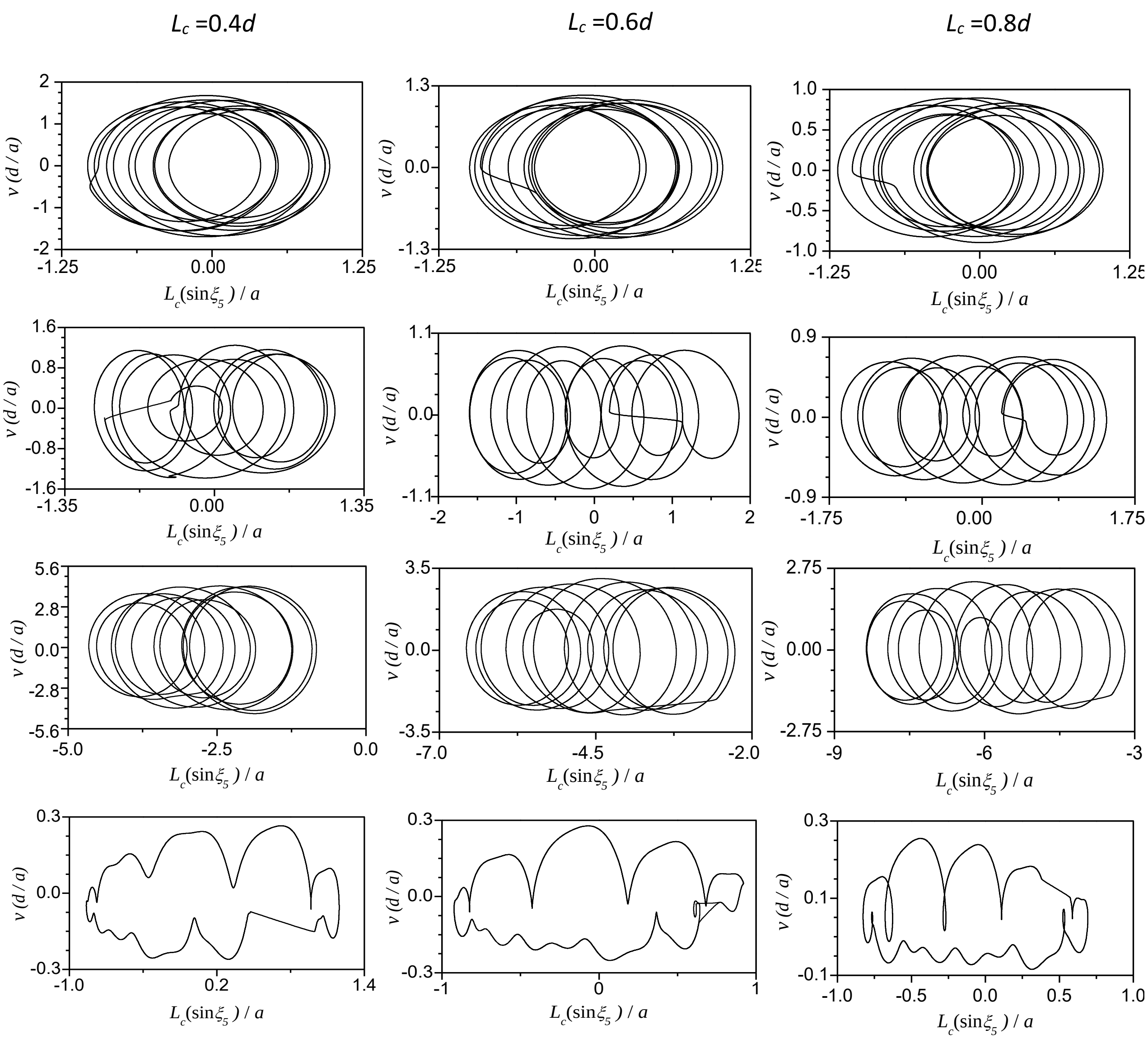

Fig. 13. Phase trajectories of payload motion for various cable lengths at a = 0.015 and ω = 2.0: row 1: Cylinder Only; row 2: Head Sea; row 3: Beam Sea Up; and row 4: Beam Sea Dn

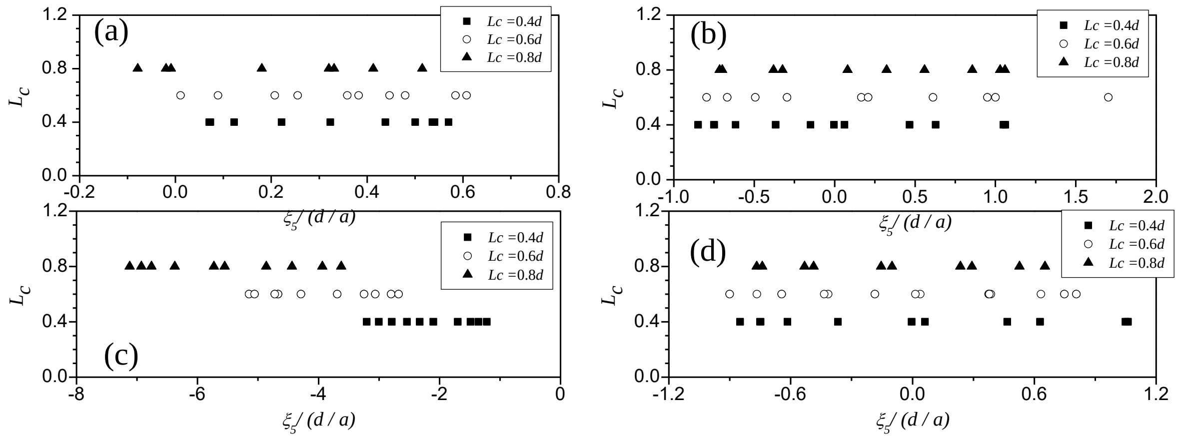

Fig. 14. Influence of cable length on dynamics of phase motions at a = 0.015 and ω = 2.0: (a) Cylinder Only; (b) Head Sea; (c) Beam Sea Up; and (d) Beam Sea Dn

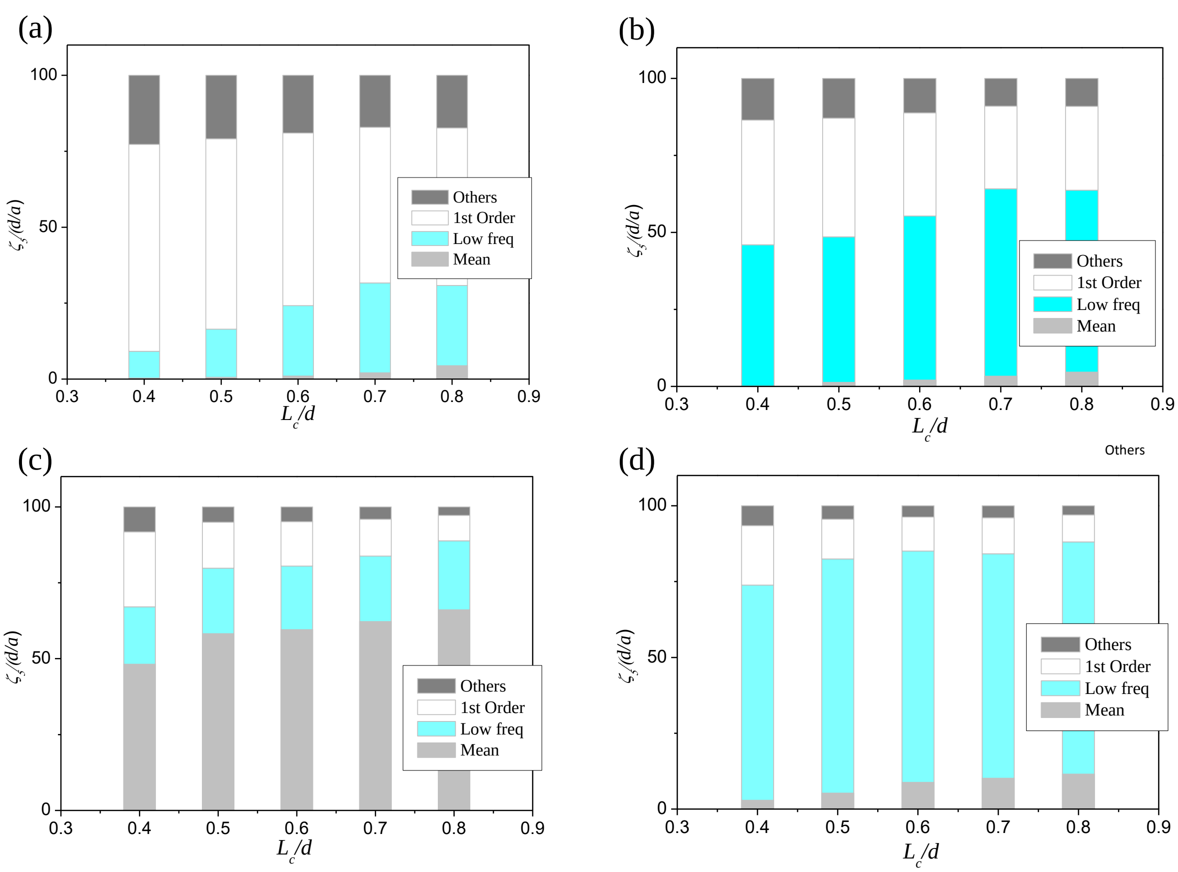

Fig. 15. Pendulum motion amplitude of the payload as percentages of various components with the variation of cable length at a = 0.015 and ω = 2.0: (a) Cylinder Only; (b) Head Sea; (c) Beam Sea Up; and (d) Beam Sea Dn

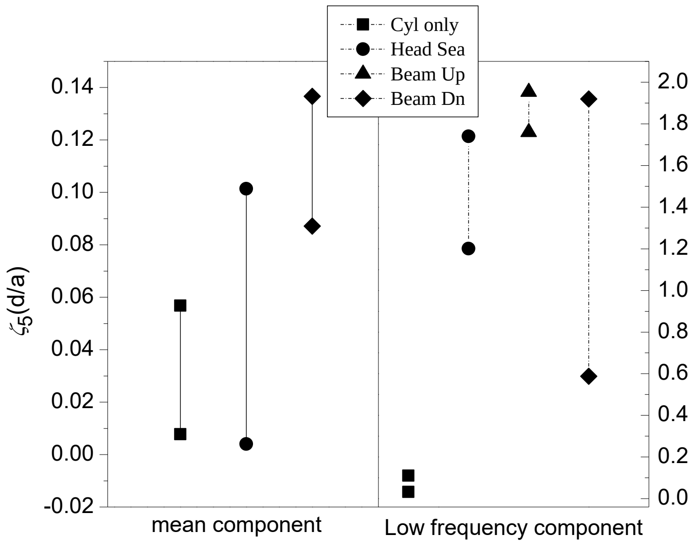

Fig. 16. Ranges (maximum to minimum) of mean and low frequency components of payload motions for cable length changes under various geometric configurations at a = 0.015 and ω = 2.0.

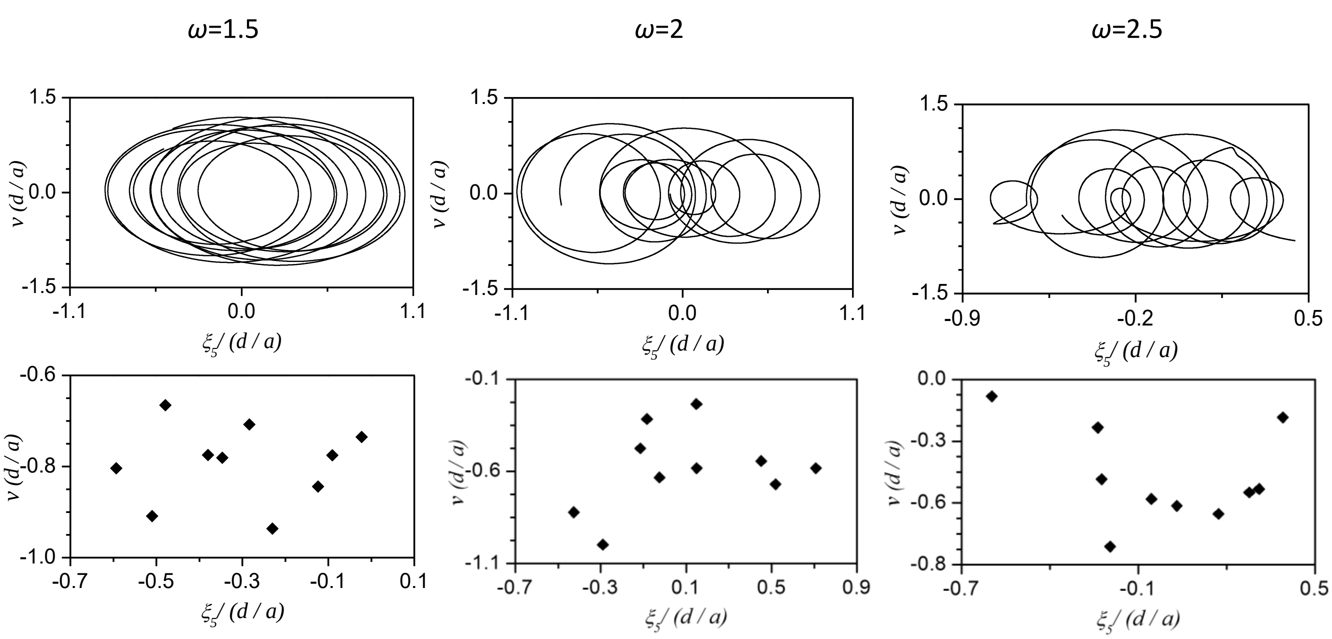

Fig. 17. Influence of wave frequency variation on the dynamics of moving downward payload at $V_d = 0.02d$, a = 0.015 [Head Sea]: row 1: phase trajectories; and row 2: Poincaré map

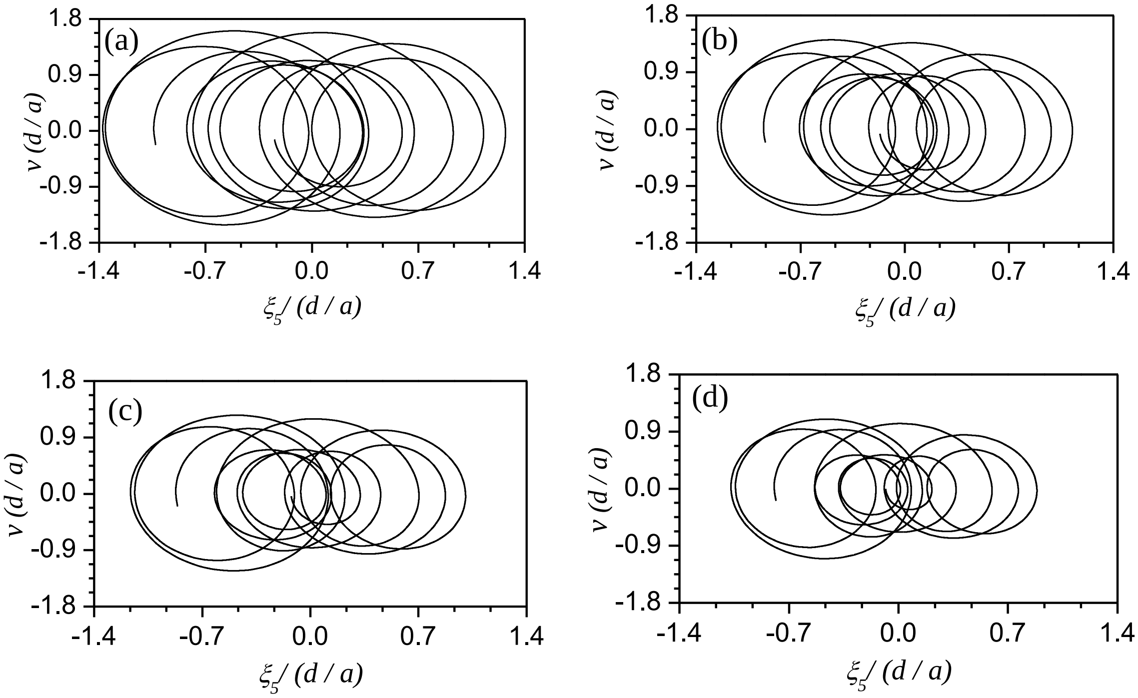

Fig. 18. Variation in the phase trajectories of the payloads due to various moving downwards speeds at $L_c = 0.8d$, $\omega = 2.0$, $a = 0.015$ [Head Sea]: (a) $V_d = 0.005$; (b) $V_d = 0.01$; (c) $V_d = 0.015$; and (d) $V_d = 0.02$

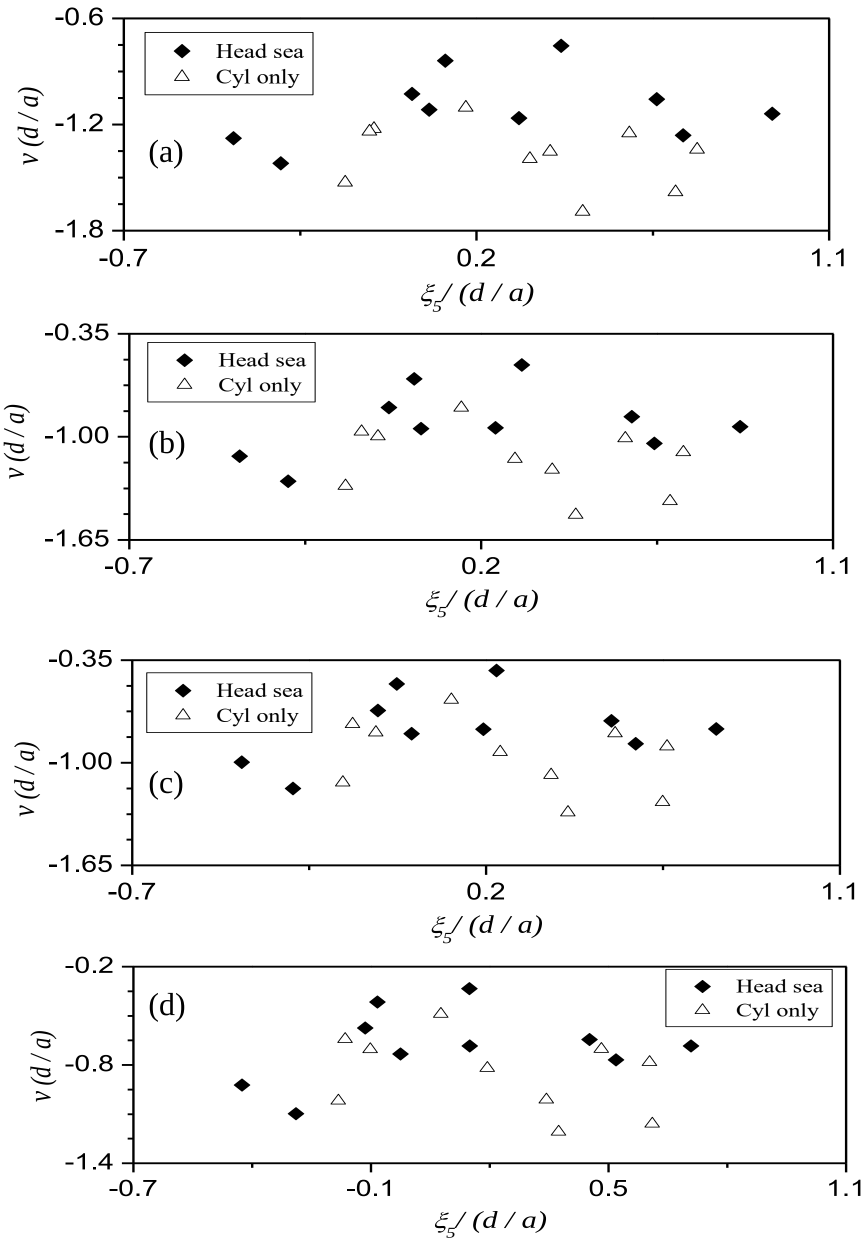

Fig. 19. Comparison of Poincaré map between the Cylinder only and Head Sea orientations of the moving downwards payload under various moving downwards speeds with L_c = 0.8*d*, ω = 2.0, *a* = 0.015: (a) V_d = 0.005; (b) V_d = 0.01; (c) V_d = 0.015; and (d) V_d = 0.02

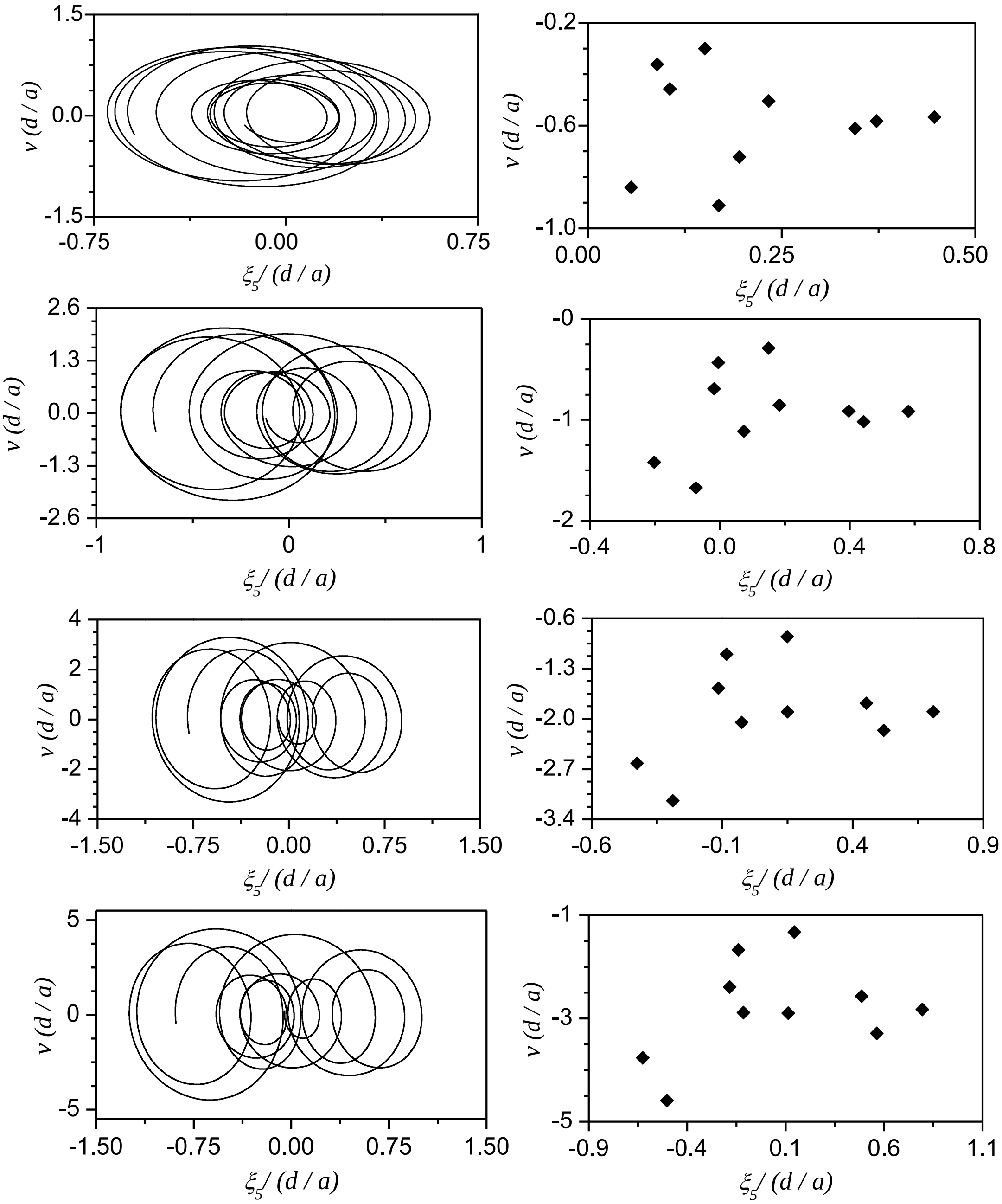

Fig. 20. Influence of various motion amplitudes of wave maker on dynamic behavior of payload moving downwards with L_c = 0.8d, ω = 2.0 [Head Sea]: column 1: phase trajectories; column 2: Poincaré map; row 1: a = 0.005; row 2: a = 0.01; row 3: a = 0.015; and row 4: a = 0.02

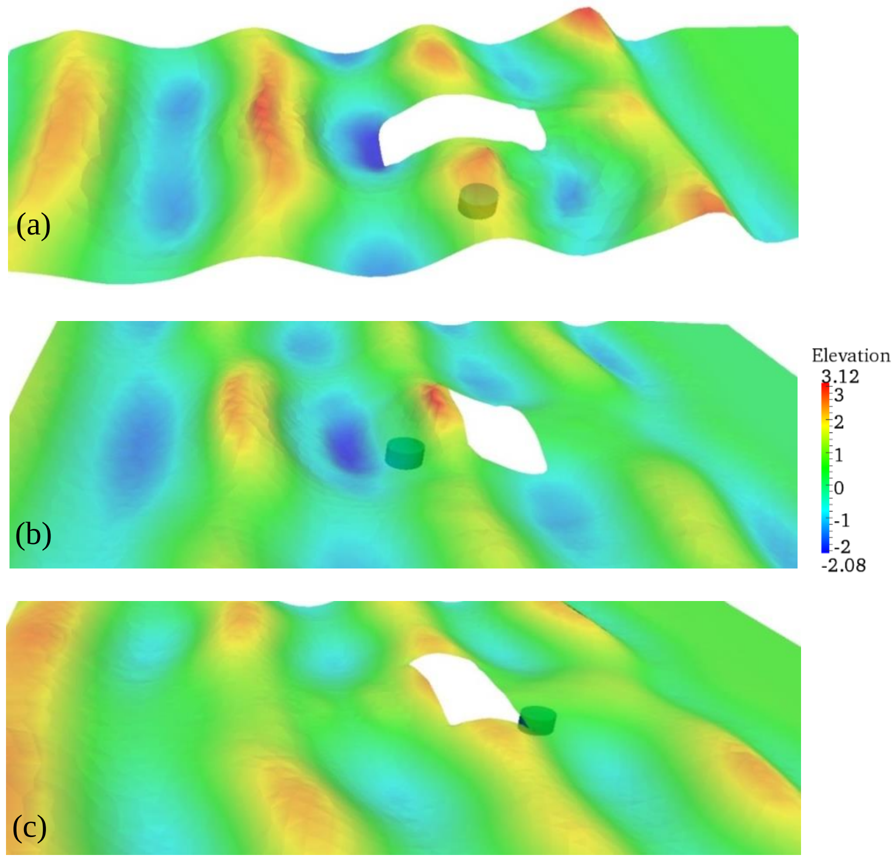

Fig. 21. Wave profile snapshots at t =9.5T with a = 0.02, ω = 2.0: (a) Head sea; (b) Beam Sea Up; and (c) Beam Sea Dn

Table 1. List of test cases

Total number of simulations	L_c/d	a	ω	D/d	V_d/d	Geometric Configuration
Nonlinear dynamics of submerged payload under various wave frequencies						
11	0.5	0.01	1.50 to 2.50, at interval of 0.1	0.2	N.A.	Cyl only
11	0.5	0.01	1.50 to 2.50, at interval of 0.1	0.2	N.A.	Head Sea
11	0.5	0.01	1.50 to 2.50, at interval of 0.1	0.2	N.A.	Beam Sea Up
11	0.5	0.01	1.50 to 2.50, at interval of 0.1	0.2	N.A.	Beam Sea Dn
Variation in payload pendulum motion dynamics for different cable lengths						
3	0.4, 0.6, 0.8	0.015	2.0	0.2	N.A.	Cyl only
3	0.4, 0.6, 0.8	0.015	2.0	0.2	N.A.	Head Sea
3	0.4, 0.6, 0.8	0.015	2.0	0.2	N.A.	Beam Sea Up
3	0.4, 0.6, 0.8	0.015	2.0	0.2	N.A.	Beam Sea Dn
Nonlinear dynamics of payload moving downwards at a constant speed						
Variation of wave frequencies						
3	0.8	0.015	1.50, 2.00, 2.50	0.15	0.02	Head Sea
Influence of moving downward speed						
4	0.8	0.015	2.0	0.15	0.005 to 0.02	Head Sea
4	0.8	0.015	2.0	0.15	0.005 to 0.02	Cyl only
Payload moving downwards under various motion amplitudes of wave						
4	0.8	0.005 to 0.02	2.0	0.15	0.02	Head Sea